Oregon State University

Final Report

Chetco River Tidal Hydrodynamics and Associated Marina Flushing

Support by
Port of Brookings
and
Sea Grant Programs
Oregon State University

L.S.Slotta, Principal Investigator
with
S.S.Tang

Ocean Engineering Programs
School of Engineering
Oregon State University
Corvallis , Oregon 97331

September, 1976

ACKNOWLEDGEMENTS:

This report contains the work presented by Shing Shirly Tang in her Master of Ocean Engineering dissertation at Oregon State University, under the direction of Dr. Larry S. Slotta.

We wish to thank the commissioners and staff of the Port of Brookings for their financial support for these studies and their personal interest is this project, especially Dot Martin, Fred Stutsman, Joe Salsia and Robert White.

A particular note of acknowledgement directed to the Sea Grant College Program for their interest and support of our project.

DISCLAIMER:

Views or conclusions contained in this report should not be interpreted as representing policy or opinion of the Port of Brookings.

LIST OF TABLES

TABLE OF CONTENTS

LIST OF FIGURES

LIST OF FIGURES (continued)

LIST OF FIGURES (continued)

ABSTRACT:

Chetco River Tidal Hydrodynamics and Associated Marina Flushing

by

Larry S. Slotta and Shing Shirly Tang

The purpose of this study was to provide an understanding of the interrelationships between fresh and salt water circulation, tidal transport and flushing patterns in the Chetco River estuary and its boat basins.

Field work and water quality measurements were conducted at the entrance of the Chetco River during 1975 and 1976. These results were used for classifying the estuary and for developing and verifying both numerical and physical models.

A one-dimensional numerical model was successfully used to simulate the tide and currents of the Chetco River. The model was calibrated prior to the recent (1976) port expansion and was used to predict the expected changes in tidal response due to the enlargement of the tidal basin. Subsequently, analytical and physical models were applied to predict the flushing ability of the new boat basin. Attempts were made to use a two-dimensional finite element numerical model for calculating currents and simulating the circulation in the boat basins. Results were compared with those taken during seasonal field studies.

Analytical models were found to be economical and effective for estimating the flushing rate in small marinas, when applied with caution. Application of numerical models to small basins seems somewhat impractical because of grid size detail and computational costs. When studying the flushing characteristics of proposed marinas, a reduced-scale physical model is considered to be a most effective tool. For prototype considerations, field studies can be most instructive in providing information for decisions regarding the flushing characteristics of marinas.

The study results show that the Port of Brookings marina flushing ranges from four to eight tidal cycles (two to four days). The new marina flushing rate depends on the range of tide and the strength of the ambient river currents. Water quality studies indicated that the Chetco River area has satisfactory water quality throughout all seasons; the only possible exception being when continuous dry summer months might occur along with high recreational use of the marina.

II. TIDAL HYDRODYNAMICS OF THE CHETCO RIVER

General Description:

The Chetco River originates in the mountains of Southwestern Oregon and flows for 93.3 kilometers (58 miles) before it empties into the Pacific Ocean. The 929.8 square kilometer (359 square mile) drainage area is mainly comprised of forests. The drainage area is sparsely populated. Brookings and Harbor are the only two towns near the Chetco River, both being located at the mouth. The combined population of this area in 1973 was 5500.

The economics of the Chetco River communities depends primarily on forestry and the manufacture of wood products. Shipping of wood products, commerical fishing and recreation are of importance at the Port of Brookings.

The river entrance is protected by a rocky headland about 24 meters high which forms the western extremity of Chetco Cove and protects the entrance from north-westerly storms and to some extent from westerly storms.

Man-made physical alterations to the river are summarized in Table I and illustrated in Figures 2 and 3. Construction projects were authorized by the River and Harbor Act in 1945 and modified in 1965; they provided for construction of two jetties at the mouth of the river, an entrance channel 4.3 meters deep and 36.6 meters wide, a barge turning basin 4.3 meters deep, a protective dike, and a small-boat access channel 3.7 meters deep and 30.5 meters wide. A small-boat basin 3.7 meters deep was provided by local interests. The demand for moorage of commercial and sport fishing boats has far exceeded most expectations. The Port of Brookings planned a new small-boat basin in 1974 which was completed and opened to the public in 1976.

Hydrology and Climatology:

The climate in the Southern Oregon Coastal Basin is very similar to the mid and northern portions of the Coastal zone, because of the influence of the Pacific Ocean. The average annual precipitation of the Basin area is lowest near the mouth with 200 centimeters (80 inches) and increases with elevation. Nearly 80 percent of this average annual precipitation occurs during the six month period of October through March, with about 50 percent during November, December and January. Precipitation during the three lowest months of June, July and August is only about 4 percent of the total annual precipitation. Monthly precipitation and temperature data are shown in Figure 4.

The average wind direction in the vicinity of the estuary is as follows: Northeast during November through March, Northwest in April, May and June, South in July and August, Northwest in September and North in October. Wind direction data are presented in Figure 5.

The seasonal runoff pattern of the Chetco River is typical of most streams in the Coastal zone in that it closely follows the patterns of

Table I. Man-made Physical Alterations to the Chetco River Estuary

Proposed Project	Location	Dimensions (in Meters) Depth	Width	Length	Height	Date Completed
North Jetty	Chetco River Mouth	--	--	381	--	1957-Complete
				137 Extension	4.9 & up	1969-Extension
South Jetty	Chetco River Mouth	--	--	479	Various	1957
					Elevation Increased	1963
Entrance Channel	Through the Bar	1.8	36.6	--	--	1959
		4.3	36.6			1969
Small Boat Basin and Barge Ship	300 meters Upstream Southern Side	3.7	100.6	--	--	--
Protective Dike	--	--	--	503	5.5	1970
Small Boat Access Channel	--	3.7	30.5	--	--	1970
Turning Basin	--	4.5	76	198	--	1970
New Boat Basin	--	3.7	168	366	--	1976

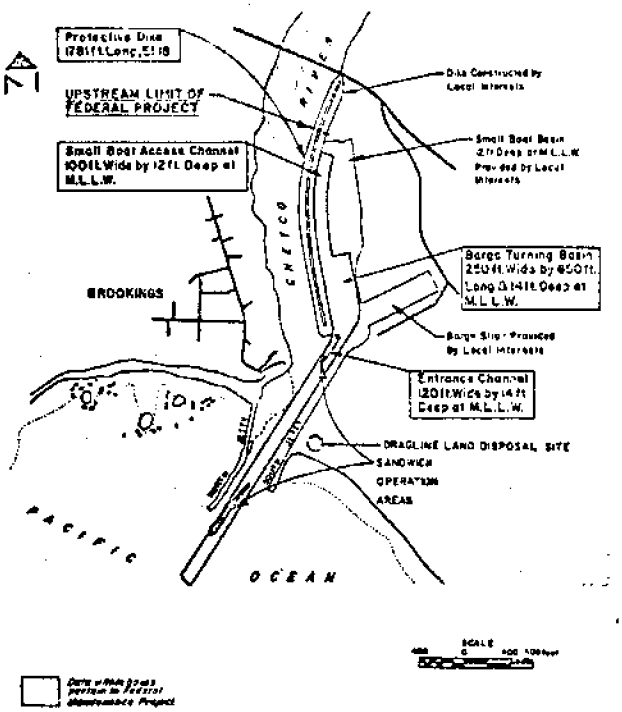

Figure 2 Chetco River Project Site (U. S. Army Engineer, Portland District 1975)

recipitation. About 90 percent of the annual yield occurs during November through April. Less than one percent occurs during August and September.

The mean monthly hydrography for the Chetco River at the mouth is based upon extrapolation of precipitation taken at Powers, Oregon from 1933 to 1972 and is shown in Figure 6. Table II lists the median monthly discharge at USGS Gaging Station #144000, river mile 10.5 Chetco River, averaged from 1970 to 1973.

Bathymetry:

Available bathymetric information of this area was obtained from the U. S. Army Corps of Engineers, Portland District (Chart CH-1-101). These data were collected to provide information regarding to channel maintenance and navigation; the soundings have been limited to the entrance channel and barge turning basin. In areas of interest where no sounding data were available, the OSU Ocean Engineering staff conducted detailed surveys of the estuary during June and July 1975. Three bench marks were used as control points. Their locations and elevations were obtained from the Port Engineer and the State Land Division. The number and spacing of bathymetry sections established depended on the complexity of the site geometry. Locations of these bathymetry sections and the cross-sections are shown in Appendix A. Side-scan sonar was also used in the lower river portion and the turning basin for reconnaissance purposes. The side-scan sonar records are also included in Appendix A.

The purpose of completing a bathymetry survey of the Chetco River was to provide information for calculating the tidal prism, schematization of the estuary to serve as input data needed in numerical modeling of the tidal dynamics, and for construction of a physical hydraulic model.

The cross-sectional areas under the low water level and the high water level, plotted against the distance upstream (from the mouth), are presented in Figure 7. The volume of water accumulated upstream under the low water and high water lines, plotted against the distance upstream, is shown in Figure 8, representing both high and low river runoff with a 1.8 meter tide. Tidal prism calculations for two cases show that the value under low river flow conditions (9.0×10^5 cubic meters) is higher than that of high river flow conditions (7.5×10^5 cubic meters). As illustrated in Figure 9, it is noted that during high river runoff the tide has less effect on the estuary and that the fresh water flow tends to be a dominant factor over tidal action. (The new Port of Brookings' boat basin project (1975-76) contributes 1.15×10^5 cubic meters (4.1×10^6 cubic feet under 6 foot tide) of water to the estuarine tidal prism. This is approximately 15 percent of the tidal prism.)

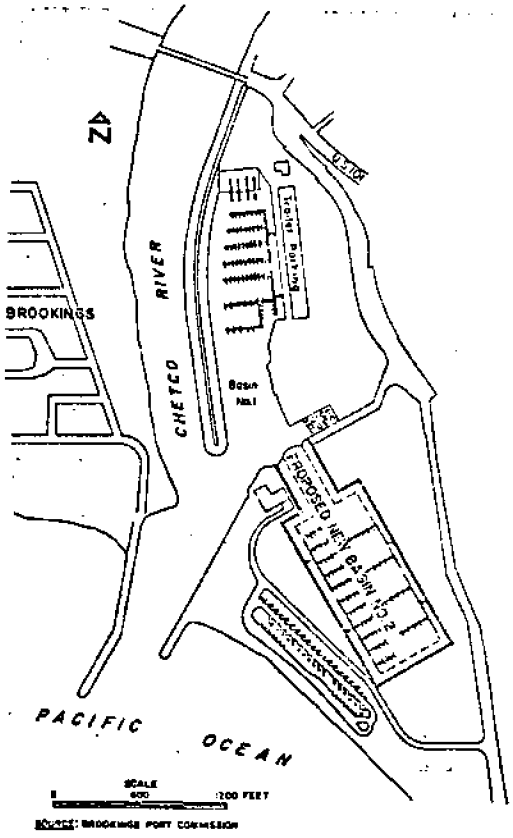

Figure 3. Proposed boat basin, Chetco River project area (Completed 1976)

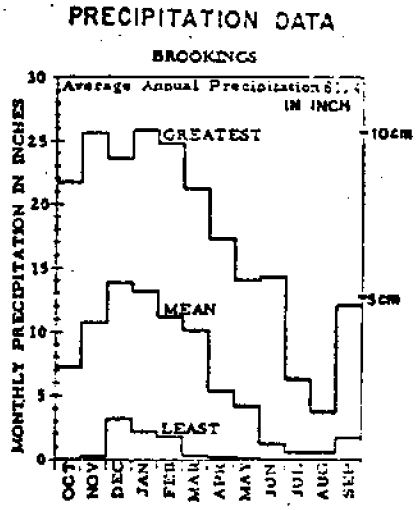

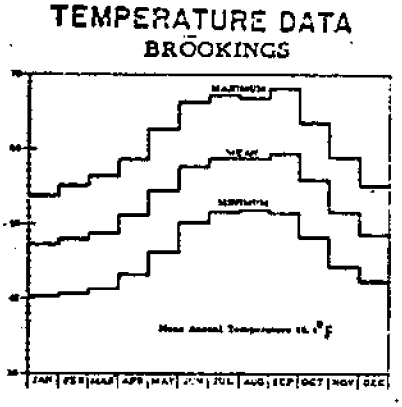

Figure 4.

Representative precipitation and temperature data: Brookings, Oregon. (Climatalogical Handbook, Columbia Basin States, June 1969).

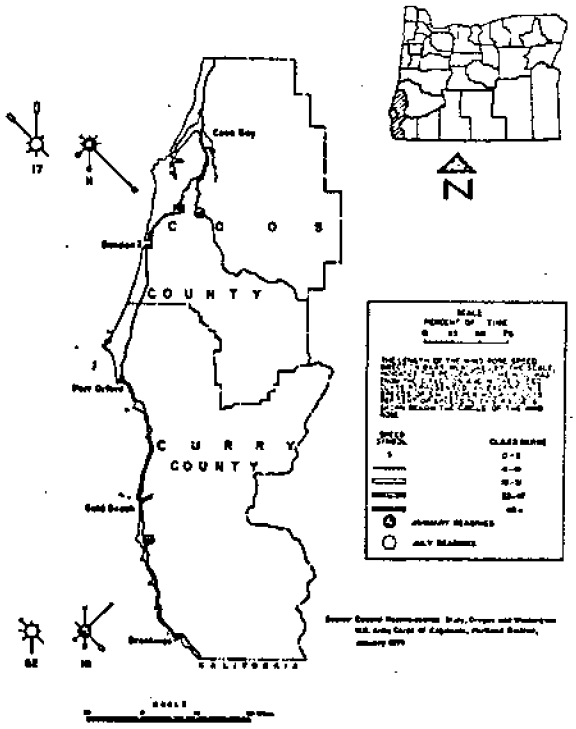

Figure 5. Representative wind direction data:Chetco Cove area.

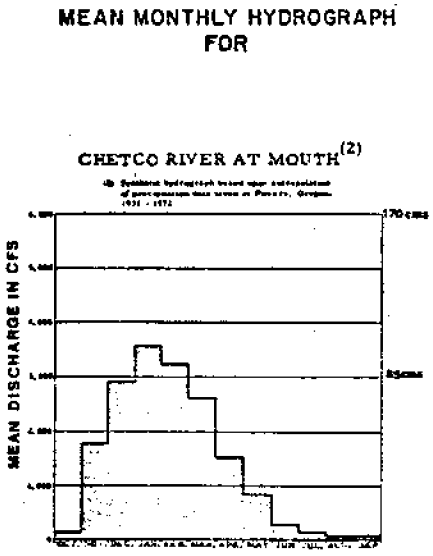

Figure 6. Mean monthly hydrograph for the Chetco River at its mouth.

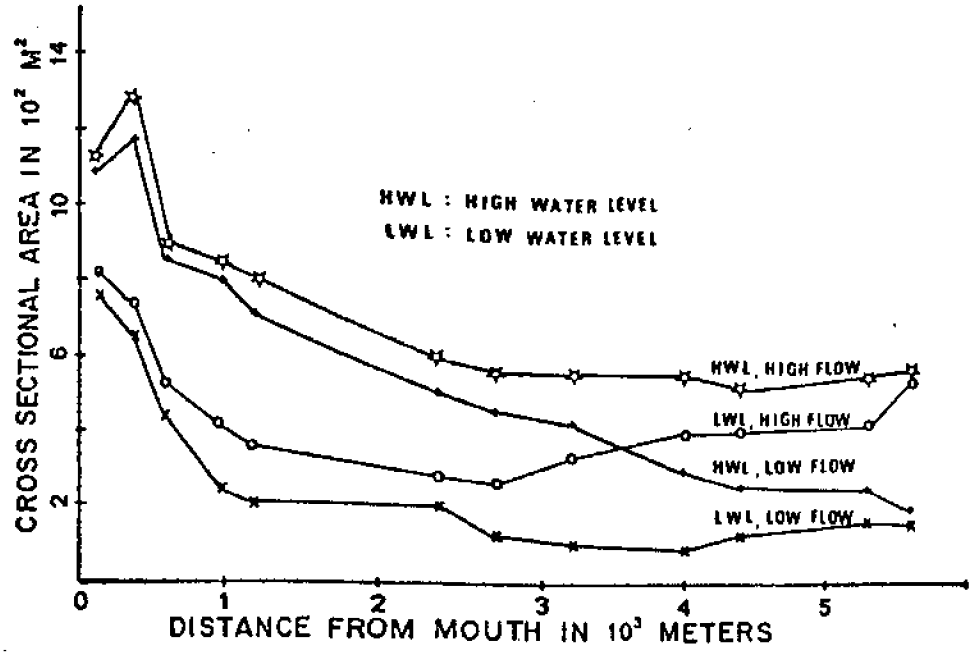

Figure 7. Cross-sectional areas of the Chetco River under low water levels and high water levels during high and low river flow conditions and a 1.8 meters tide.

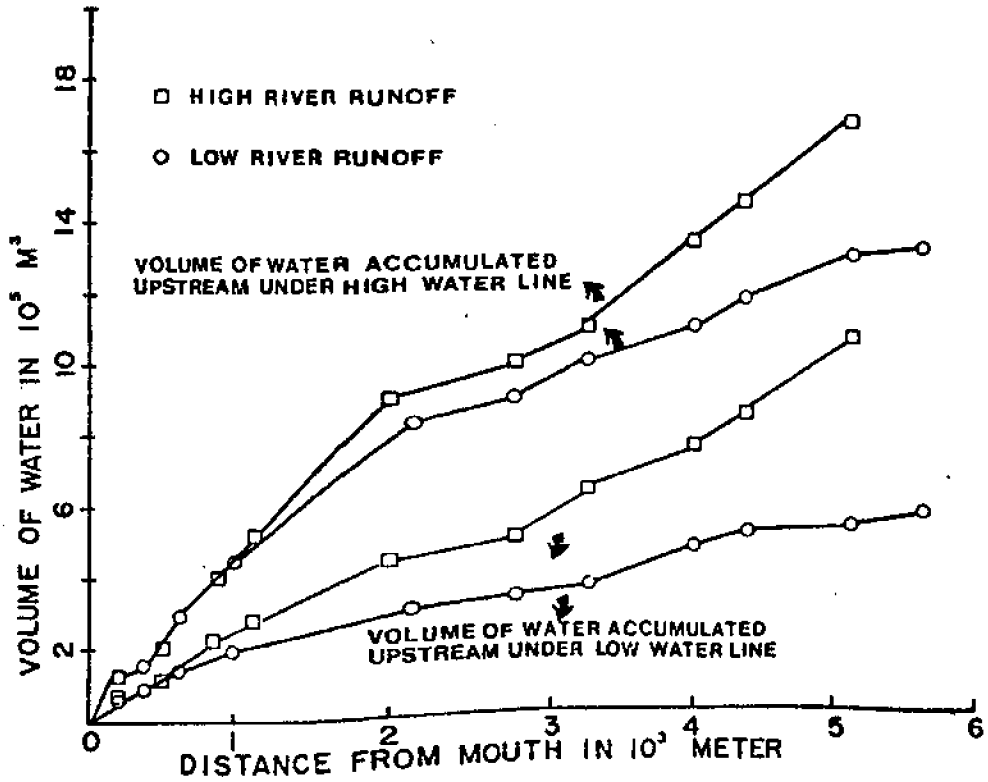

Figure 8. Volume of water accumulated upstream under LWL and HWL during high and low river flow conditions and a 1.8 meters tide.

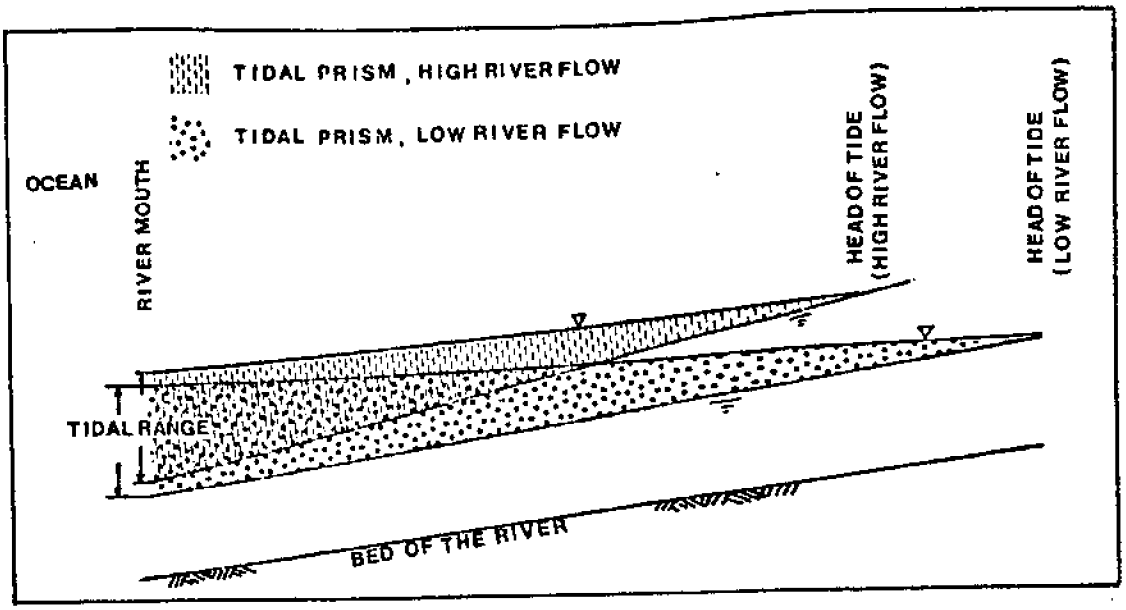

Figure 9. High and low water levels in the Chetco River under high and low river flow conditions.

Table II. Median Monthly Discharge Near the Mouth of the Chetco River

MEDIAN MONTHLY DISCHARGE IN m^3/s

	Years of Record	Oct.	Nov.	Dec.	Jan.	Feb.	Mar.	Apr.	May	Jun.	Jul.	Aug.	Sept.	Annual
(1)	38	4.53	51	83.5	102	105	74	44	23	7.6	3.1	1.7	1.7	41.8
(2)	3	16.3	121	257	166	164	223	99	43.5	17.7	8.6	5.2	6.3	94.1

Sources:

(1) - J. Duggan, Planning Branch, Oregon State Water Resources Board, Salem, Oregon.

(2) - USGS Gaging Station near Brookings, Oregon 1970-1973.

Tidal Dynamics:

The tides in Chetco Cove are classed as the "mixed semi-diurnal" type, with a marked variation between the two high tides and two low tides that occur daily. The normal sequence is shown in Figure 10. The combined effects of the sun and the moon's relative positions cause bi-weekly tidal variations. (Spring tides occur when the sun and the moon are aligned (full and new moon) and their forces are additive. The neap tide occurs when they are 90 degrees out of phase (first and third quarter).

Daily tide preditions at Humboldt Bay, California are published annually by the National Ocean Survey (NOS) (Tide Table, West Coast of North and South America 1975, 1976). Predictions of tides at the Chetco River mouth can be obtained by applying tide and time differences referenced to the NOS predictions for Humboldt Bay, California. High tides arrive on the average 30 minutes earlier and stand an average of .15 meters higher, and low tides are 26 minutes earlier and are the same height as those at Humboldt Bay. The mean range is 1.56 meters (5.1 feet) with a mean tide level of 1.13 meters (3.7 feet) above Mean Lower Low Water (MLLW) level.

After tides enter a well defined boundary area such as in a tidal river, bay, etc., there are a number of factors that govern the tidal motion in the basin, such as:

1) estuary geometry
2) boundary roughness
3) fresh water discharge at the river head
4) fresh water inflow from side channels or ground water seepage
5) meteorological conditions
6) coriolis effects
7) coastal processes and coastline features near the estuary's entrance

All of these factors combined together could make the tide propagation in the estuary a rather complicated problem. Nevertheless, some of the factors have such little effect on the whole estuarine system that they can be neglected. The Chetco River, for example, is long and narrow (comparing its length to width). For a given discharge, little lateral variation of water surface elevation and current direction has been observed. This estuary can indeed be described as being one-dimensional, where basin geometry, boundary condition and fresh water inflow are dominant factors provided that no dramatic hydrologic flow variations are experienced.

In order to be able to predict the effect on the tides and currents after the port expansion, a numerical model application was considered, since it would be impossible to measure tides and currents throughout the estuary under all seasonal combinations of river flow and bay mouth tides.

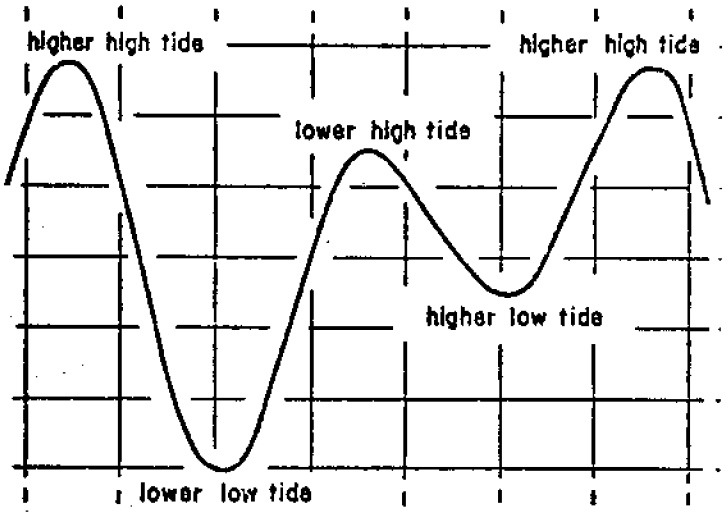

Figure 10. Typical mixed semi-diurnal tide.

One-Dimensional Numerical Model Application:

A one-dimensional numerical program developed by Harleman, Lee and Thatcher (Harleman, et. al., 1969 and 1973) was selected for examining the tidal flows and currents of the Chetco River. The program is based on one-dimensional continuity and momentum relationships which are solved simultaneously by means of an explicit finite-difference scheme. Output from the program consists of a listing of cross-sectional averaged flow rates and tidal levels as a function of time. A plotting routine developed at Oregon State University presents the output in graphical form showing the tidal level and flow rate versus time for given stations (tidal elevation for odd stations, flow rate for even stations).

Two basic assumptions were made in the program formulation. First, it was assumed that the driving force of the system would be the periodical rising and falling of the water surface at the mouth of the estuary. Second, the tides were assumed to be a shallow water wave with a long period (12.4 hours), since the water depth in the Chetco River is relatively small (1 to 5 meters) compared to the wave length (approximately 3×10^9 meters). To apply the numerical program, the required information consists of: input tidal data at the mouth, river inflow, and geometry of the waterway. After schematizing the estuary into a discrete number of sections with respect to a known datum, and specifying the boundary conditions, the program can be run.

Tidal recordings at the Chetco entrance obtained from field trips on February 8 and 9, 1975 and June 18 and 19, 1975 (Figure 11) were used as the input tides. River inflow was averaged at 396 m^3/s (14000 cfs) on February 8 and 9, and 8.5 m^3/s (300 cfs) on June 18 and 19, 1975.

The Chetco River was then divided into six segments on a 3600 foot spacing shown in Figure 12. The cross-section of the river was represented by a rectangular core area where the flow process takes place; the boat basins were simulated by a side rectangular area which functioned only as storage. Bathymetric surveys conducted during June and July 1975 provided the necessary information for schematization. A summary of the Chetco River schematization is listed in Appendix B.

The explicit finite-difference solution of continuity and momentum equations imposed a limit on the time increment Δt which was approximated by

$$\Delta t \leq \frac{x}{u+c}$$

where x = segment length
u = average cross-sectional velocity
c = wave speed = $\sqrt{gd}$
g = gravitational acceleration
d = average depth of the river.

Δt was chosen as 100 second in the Chetco River numerical model in which the number of time steps for a typical day's tide is 880.

The computer program was then run with an arbitrarily selected initial condition $\eta(x,0) = Q(x,0) = 0$, (x measured from the mouth). After the computer generated a few cycles, a stable condition of tides and currents was achieved.

Numerical Model Calibration:

To be able to calibrate the numerical model, field measurements are essential. Field activities undertaken by the OSU Ocean Engineering staff for the purpose of developing and calibrating numerical and hydraulic models are summarized in Table III; also refer to Figure 12 regarding the locations of tide and current stations. These stations were chosen to coincide with the stations of the numerical model schematization. (Tidal recording and river current measurements were obtained during February 7 to 9, and June 17 to 19, 1975). Two types of tide gauges, Leupold and Stevens Type F Water Level records and Bristol Bubbler Tide Guage, were used. The Leupold and Stevens Water Level recorders are equipped with a float inside a stilling well whereby a chain moves with the float and drives a pen in the recorder. The bubbler gauge is a pressure sensing device with an orifice placed under water and pressurized with a nitrogen gas supply. The water pressure at the orifice is transmitted through a nitrogen gas line to a temperature compensating bellows which drives the recording pen. Both types of gauges were found to be accurate within five minutes in time and 0.03 meters in range.

Two types of current meters were used in the field: the Price cup type meter (Gurley Instruments Model No. 665E) and a Savonius Rotor Meter (Hydroproducts Model No. 460). The cup current relates speed directly but gives no directional information. The Savonius Rotor Meter not only measures the current, but also indicates the direction of flow. At each current station, the cross-section taken was perpendicular to the direction of the river flow and was divided into several measuring points. Vertical velocity profiles were subsequently taken at each point. With the cross-sectional velocity profiles and bathymetric data the discharges at each station were calculated. The velocity profiles taken at each current station were used to calculate the actual flow rate. Average velocities were obtained by dividing the actual flow rate by the associated cross-sectional areas and these were considered to be the actual averaged velocities.

It would have been desirable to have measurements during a complete tidal cycle; however, due to manual operation restrictions (mainly darkness) only part of the measurements could be obtained. The field measurements were scheduled so that the peak flows were observed.

The Chetco River computer model was then calibrated by varying the channel roughness in terms of Manning's coefficient n to achieve the best fit with the available field data. A Manning's coefficient equal to 0.025 for the entire river provided satisfactory simulations of tides and flows.

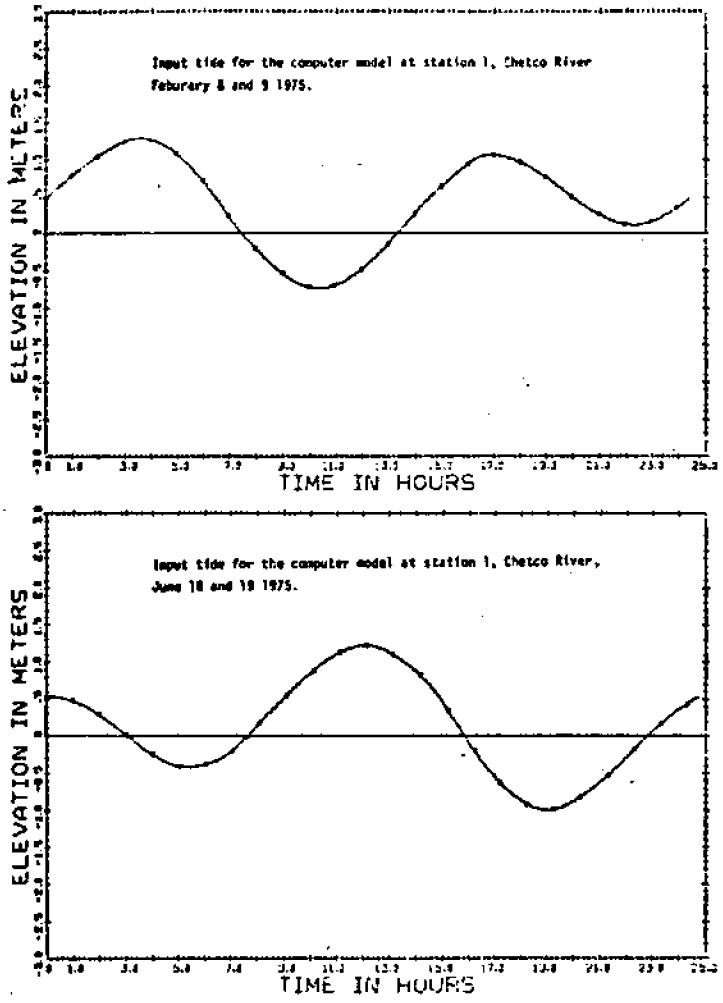

Figure 11. Input tide for the computer model at station 1, Chetco River, February 8 and 9, and June 18 and 19,1975.

Table III Summary of Field Activities in Chetco River undertaken by OSU Ocean Engineering Staff During 1975/76

	Tide Measurement		Current Measurement		Water Quality		Others	
Date	Location	Type of Gauge/ Recording Period	Location	Type of Gauge/ Period	Location &	Method	Type	Equipment
Feb 7-9 1975	South Jetty by C.G. Station	NOAA Bubbler/ Feb 7-9	4 Stations*	Price Type, Curley Meter Feb 8-9	Entrance to existing basin	Hydrolab Feb 8-9	Cross-sections Fig.	
	Snug Harbor	NOAA Bubbler Feb 7-9	Entrance to existing	Savonius Feb 8-9	Stations See Fig.	Bottle Samplers	Bottom Drifter	
	End of existing basin	Leupold & Stevens Feb 7-9						
June 17-19 1975	C. G. Station*	NOAA Bubbler June 17-19	1/2 R.M.	Savonius June 17-19			Bathymetry Survey	
	Snug Harbor*	NOAA Bubbler June 17-19						
July 11-13 1975							Bathymetry Survey	Transit Sounding Pole Boat
Sept 15-19 1975	End of existing basin	Leupold & Stevens Sept 15-16	Entrance to existing basin	Savonius	Stations	Bottle Samplers Sept 18	Muds Sample	
Jan 19-21 1976	C. G. Station	Leupold & Stevens Jan 19-21	Entrance to new basin	Price-type Curley Meter Jan 20-21	Stations	Bottle Samplers	Drogue Study	
	End of new boat basin	Leupold & Stevens (N.G.)			Entrance to new basin	Hydrolab Jan 19-21	Dye Study	Rodamin W.T.
Sept 2 1976	End of new boat basin	Leupold & Stevens	Entrance to new basin	Savonius	Both boat basins & at Chetco River	Hydrolab & Bottle Samples		

* Note Figure 12 for Station Location

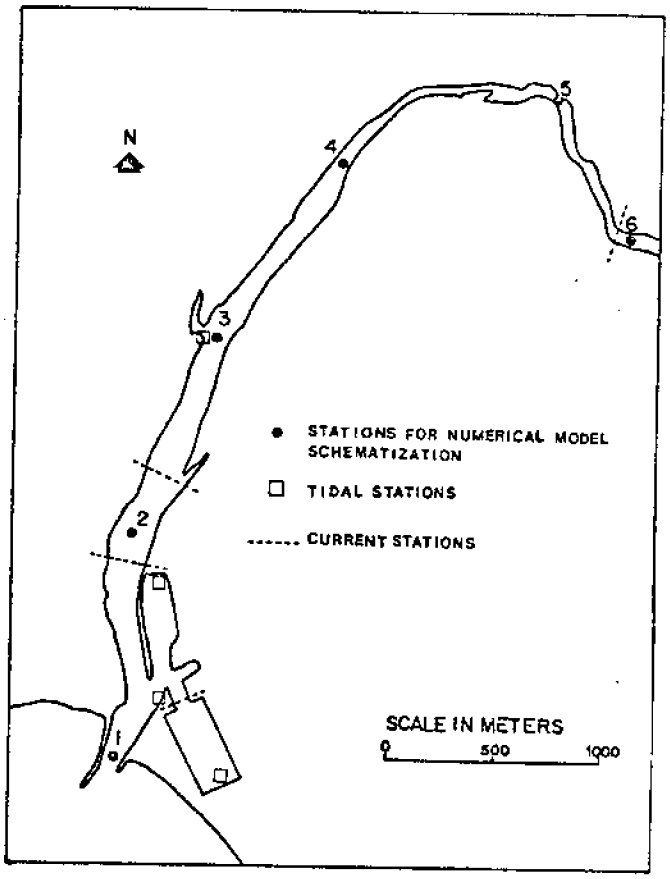

Figure 12. Schematization of the Chetco River for computer model and location of tidal and current stations.

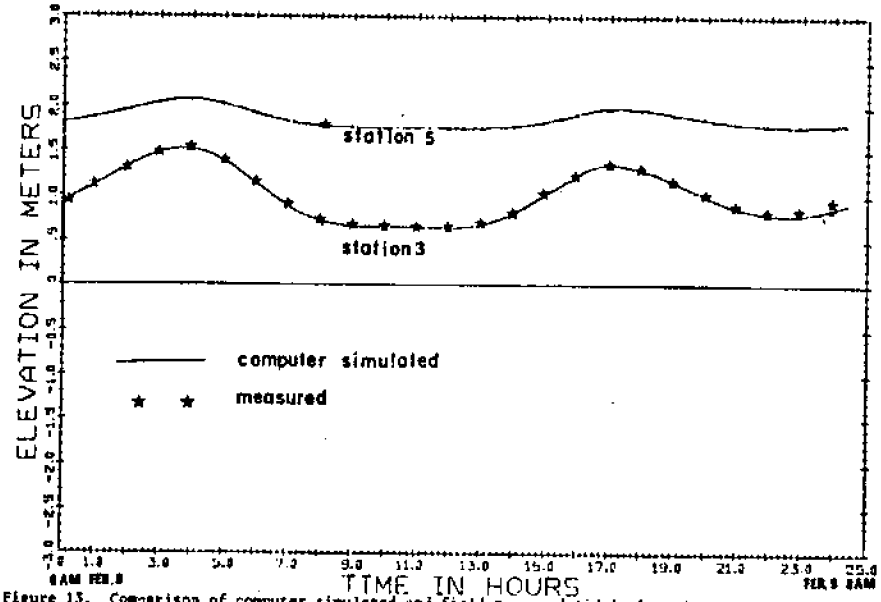

Figure 13. Comparison of computer simulated and field measured tidal elevation at station 3 and 5, Chetco River, February 8 and 9, 1975.

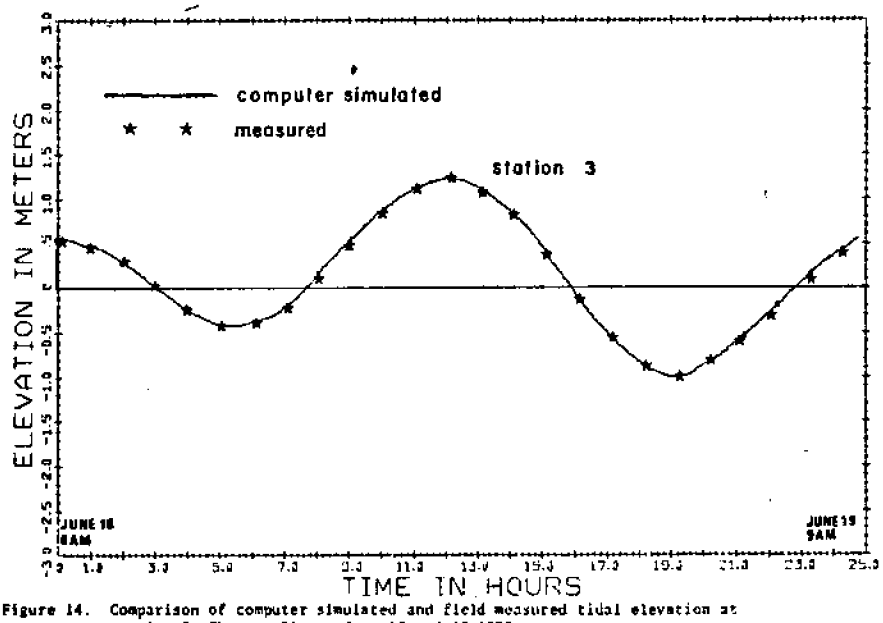

Figure 14. Comparison of computer simulated and field measured tidal elevation at station 3, Chetco River, June 18 and 19,1975.

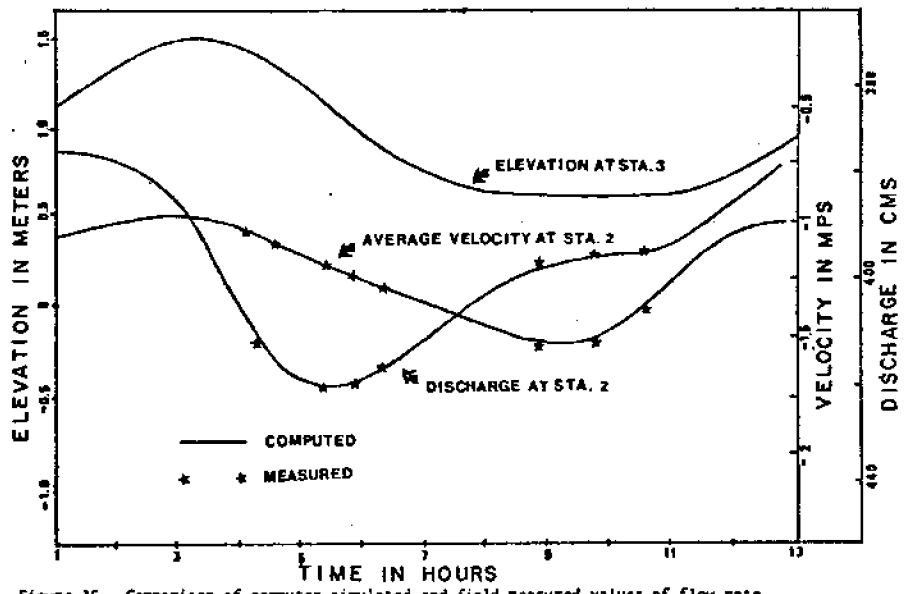

Figure 15. Comparison of computer simulated and field measured values of flow rate and average velocity for the Chetco River, February 8 and 9 with river inflow 397 m^3/sec..

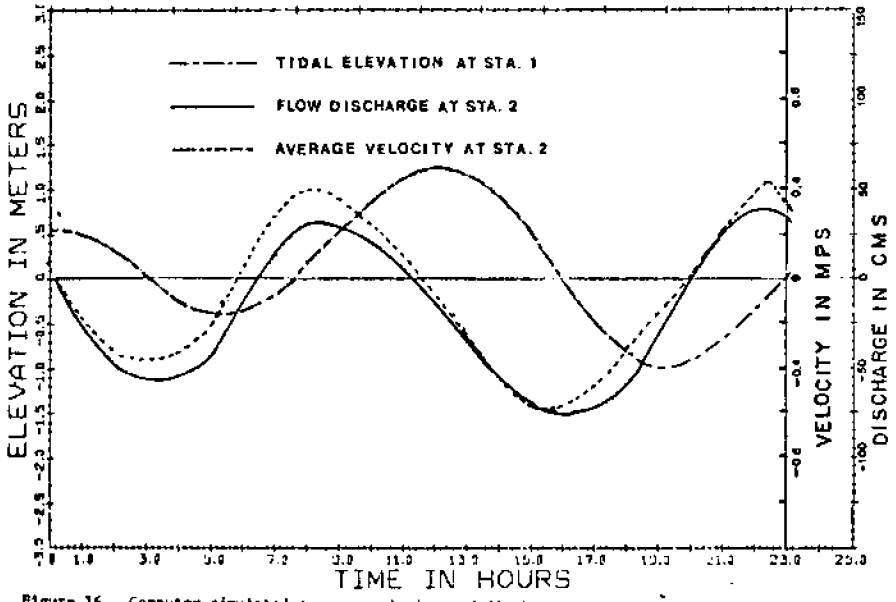

Figure 16. Computer simulated average velocity and discharge at station 2 and tidal elevation at station 1 at the Chetco River , June 18 and 19, 1975 with 85 m^3/sec. river runoff.

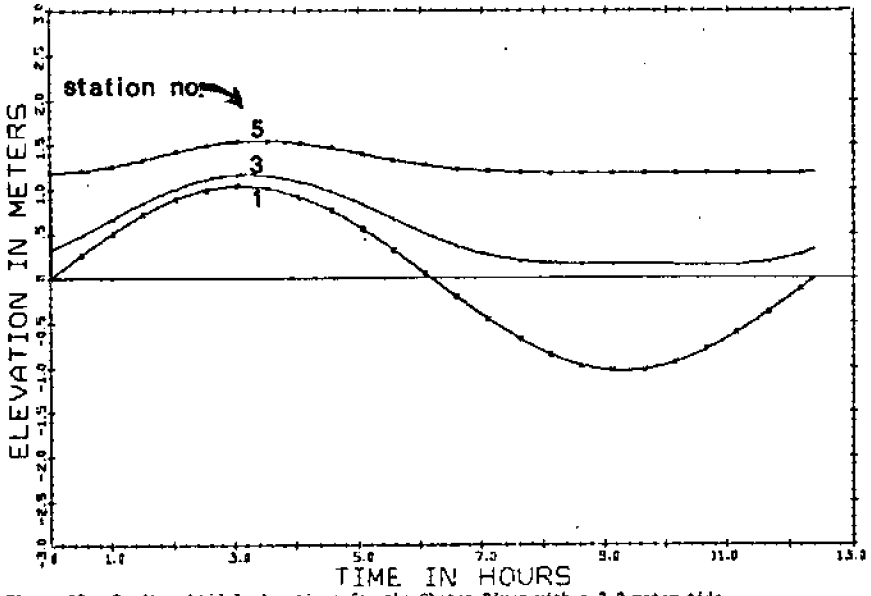

Figure 17. Predicted tidal elevations for the Chetco River with a 2.0 meter tide and 255 m^3/sec. river inflow.

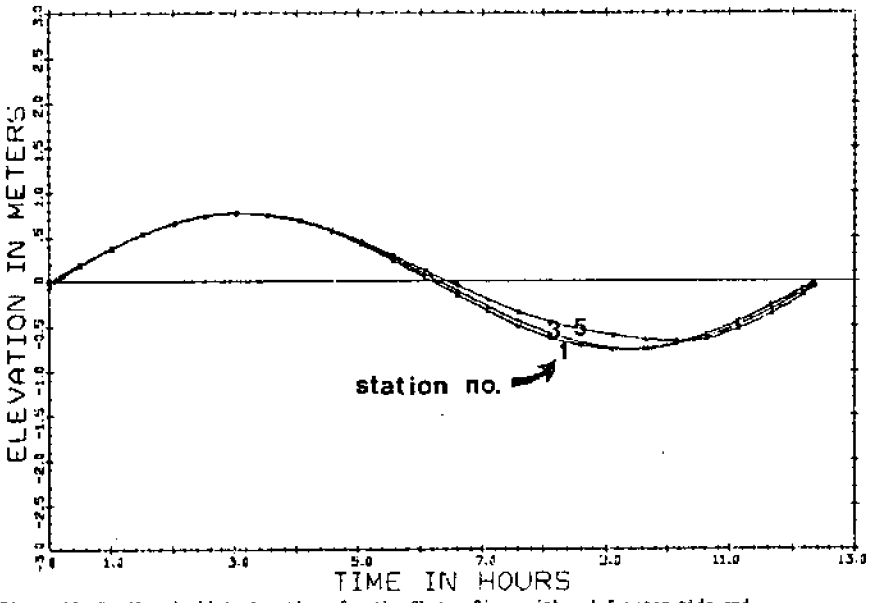

Figure 18. Predicted tidal elevations for the Chetco River with a 1.5 meter tide and 5.7 m^3/sec. river inflow.

Comparisons of measured tides and computer calculated tides for stations 3 and 5 on February 8 and 9 as well as for station 3 on June 18 and 19, 1975 are shown in Figures 13 and 14, respectively. The tidal curves show a close match between calculated and measured values.

Computer-simulated average velocities were also determined by dividing the numerically produced flow rates by the interpreted cross-sectional areas. The comparisons of actual flow rates and actual velocities with those from computer output for February 8 and 9 are shown in Figure 15. The current measurements on June 18 and 19, 1975 were unfortunately insufficient for flow rate calculations. However, a Savonius current meter located at the center of Station 2 recorded the current at mid-depth from June 18 to 19. The recording indicated that the current was weak, with a magnitude in the range of +0.3 meters/second (minus indicates downstream direction). This range corresponds to that of the computer simulated average velocity plotted in Figure 16. The velocities and flow curves are not perfect matches. There are some uncertainties in field measurements and in the interpretation of cross-sectional areas both in the field and computer program. However, it is felt that these differences are within the range of experimental accuracy.

After the computer model was calibrated to reproduce past events, it was thought reasonable that it could be used to simulate tides and currents in the same system under different boundary combinations or changes of regime. The task was to study whether there would be a significant change in tidal dynamics due to the addition of a new volume of exchanging water as represented by a large tidal storage volume (15% of the total tidal prism). Two sets of boundary conditions were selected for comparison purposes, one having a low river inflow (5.7 m^3/s) with a 1.5 meter tide and the other having a high river inflow (255 m^3/s) with a 2.0 meter tide. Each set was run with and without the port expansion (without an added storage area at Station 1).

The results revealed that the boat basin expansion does not affect the upstream tidal elevations or expand the tidal exchange. Figures 17 and 18 show the predicted tidal elevations at river inflows of 255 and 5.7 m^3/s, respectively. Figure 19 shows the predicted flow rates at a river inflow of 255 m^3/s, and the interpreted average velocities for Stations 2 and 4. Computer-predicted flow rates at Stations 2, 4 and 6 for 5.7 m^3/s river inflow are shown in Figure 20. Only the results after the expansion are shown, for there was no difference in conditions as a result of basin expansion.

Since the computer program only calculated flow rates at even numbered stations, the flow changes at Station 1 were untenable. This difficulty could be overcome if Station 2 were placed in the schematization downstream from the boat basin. However, in this case the stability requirement of the computer program would be hard to fulfill and the required computer time would be tremendous. An alternative which locates the same expansion at Station 3 with boundary conditions of a 5.7 m^3/s river inflow and a 1.5 meter tide was run. The results, when compared to those without expansion, indicated that the expansion had little effect on the tidal elevation but caused an increase in the flow rate at Station 2. Comparisons of the calculated flow rates and average velocities at Station 2 for these conditions are shown in Figures 20 and 21.

Subsequently, it can be concluded that the flow velocity at Station 1 were increased due to the port expansion at Station 1. However, it is difficult to quantify exactly the effects of the flow increase using the present numerical model.

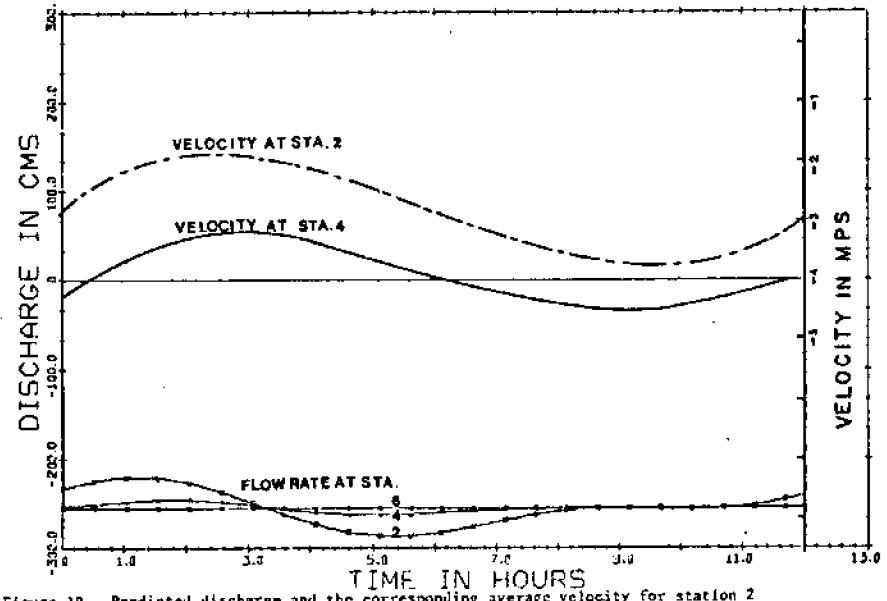

Figure 19. Predicted discharge and the corresponding average velocity for station 2 and 4 at the Chetco River . The river inflow was 255 m^3/s. and the tide had a 2.0 meter range.

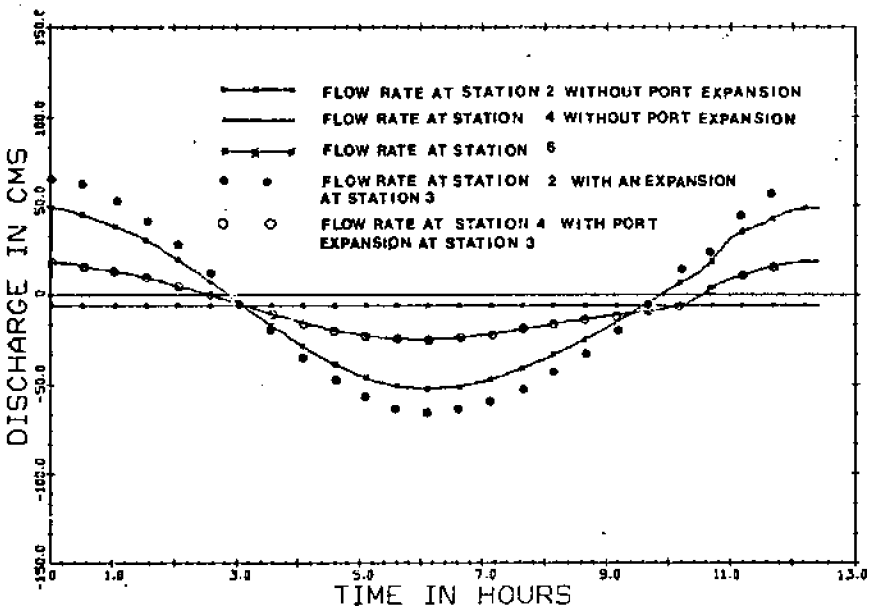

Figure 20. Comparison of computer predicted discharge at station 2 and 4 ,Chetco River with and without port expansion sited at station3.

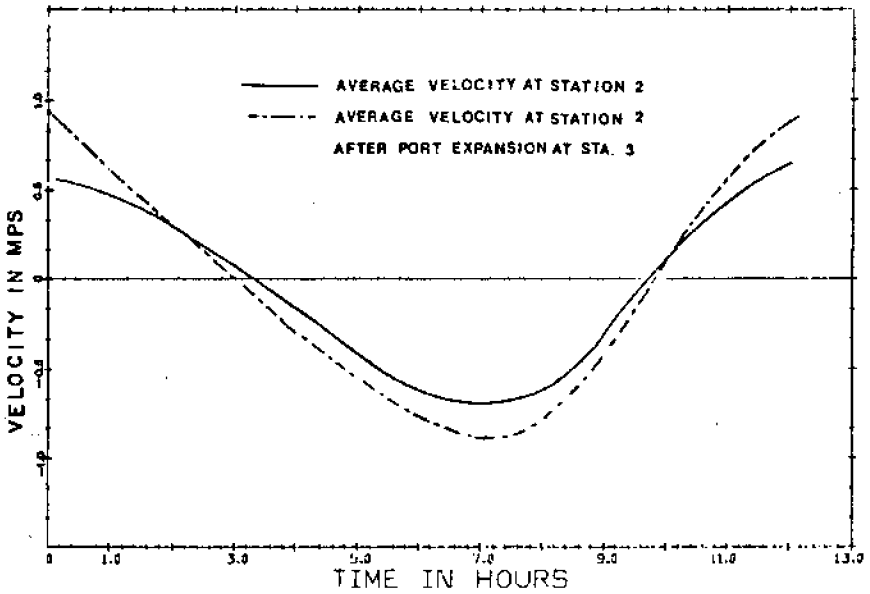

Figure 21. Comparison of computer predicted average velocities at station 2, Chetco River with and without a port expansion added at station 3.

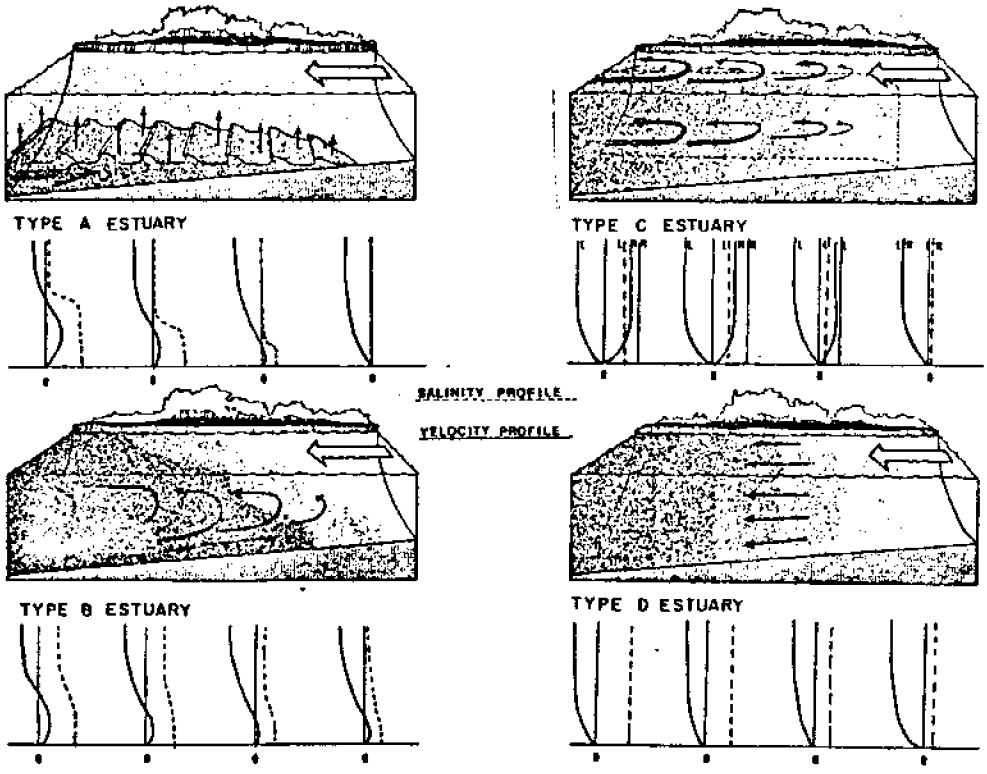

Figure 22. Four types of esturine circulation and their velocity and salinity distribution.

Estuarine Classification:

In order to compare different estuaries, it would be helpful to have a general framework from which it would be possible to predict the characteristics of similar estuaries. Thus, a scheme of estuarine classification is desirable.

A topographic classification presented by Pritchard (1967), which divided estuaries into four groups: coastal plain (drowned river valleys), fjord, bar built estuaries and the rest (estuaries not included in the first three categories). Coastal plain estuaries were formed some time following the glacial period when the sea level rose and flooded the valleys. They are generally restricted to temperate latitudes where though river flow may be large at times, the amount of sediment discharged by the river into the estuary is relatively small. In coastal plain estuaries, river flow is generally small when compared with the volume of tidal prism.

Fjords were carved by glaciers and generally have a shallow sill which was formed at the mouth by glacial deposits. The basins inside the sill are often quite deep. River discharge is small compared to the total fjord volume, but is often large with respect to the tidal prism. The occurrence of fjords is generally restricted to high latitudes in mountainous areas.

Bar-built estuaries were formed by sand islands and spits being built above the sea and extending between headlands. These can be broken y one or more inlets. Sedimentation is characteristic of this type of estuary. The position of the mouth may vary considerably from year to year. They are usually found in tropical areas or in areas where there is active coastal deposition of sediments.

The fourth category is a catch-all classification for estuaries not clearly included in the other three divisions. Included are tectonically produced estuaries: estuaries formed by faulting, landslides and volcanic eruptions.

From the geological standpoint, the Chetco estuary is classified as a coastal plain estuary.

The geomorphological classification aids us in understanding the configuration and physical characteristics of the gross circulation and its impact upon the distribution of salinity within the estuary.

Pritchard (1955) subdivided the coastal plain estuaries into four principle types: Types A, B, C and D (illustrated in Figure 22). These types differ by the character of the circulation pattern, the intensity of vertical stratification and in the extent of lateral homogeneity.

In the Type A estuary, a salt water wedge extends under the seaward flowing upper layer. The greater the river flow, the further downstream the edge of this wedge occurs. The circulation pattern is dominated by the river flow. Tidal mixing is relatively unimportant in this type of estuary.

In the Type B estuary, tidal mixing plays an important role in the circulation. Mixing occurs between the upper, seaward-flowing layer and the lower layer of higher salinity water flowing up the estuary along the bottom.

In the Type C estuary, the tidal velocities are strong enough to cause vertical mixing so that the estuary becomes vertically homogenous. The salt balance can no longer be maintained by a vertically stratified flow, and instead a lateral flow pattern is effected by the earth's rotation. Lateral advection and lateral eddy mixing of salt take place in this type of estuary.

In the Type D estuary, the tidal mixing is sufficient to destroy the lateral salinity gradient and to produce vertical saline homogeneity. The salt balance is maintained by a balance between the longitudinal flux of salt out of the estuary by advection and the longitudinal flux of salt into the estuary by longitudinal mixing.

In Pritchard's classification, the important physical parameters which are considered to control the sequence of shifts of estuarine type are: the river flow, the tide, the mean depth of the estuary and the width of the estuary. These factors change from time to time or even from section to section within an estuary. Thus the estuary behavior or characterization can change accordingly. Pritchard recognized that other external factors, such as wind velocity, air temperature, solar radiation, and bottom roughness also play a part in controlling the vertical saline stratification and the circulation characteristics, but are negligible under normal conditions.

Several parameters have been developed for classifying estuaries. A very general criteria which does not include either estuary shape, width, or depth has been suggested by Simmons (1955). This is the flow ratio, defined as the ratio of river flow per tidal cycle to tidal prism. When the flow ratio is greater than 1, the estuary is highly stratified (Type A), whereas a flow ratio of about 0.25 may indicate a partially mixed system (Type B). Flow ratios less than 0.1 tend to describe a well mixed condition (Type C or D).

Burt and McAlister (1959) devised another method based on the difference between surface and bottom salinities at the station where the mean salinity is closest to 17 ppt. If the salinities difference is greater than or equal to 20 ppt, the estuary is stratified (Type A). A difference between 19 ppt and 4 ppt indicates a partially mixed estuary (Type B). If the difference is less than 3 ppt, the estuary is well-mixed (Type C or D).

Ippen and Harleman (1966) have developed another classification method according to a stratification number G/J. The ratio G/J is a measure of the amount of energy lost by tidal waves relative to that used in mixing the water column. Increasing the values of the stratification number indicate increasingly well mixed conditions, and low numbers represent highly stratified conditions. This method requires rather precise tidal elevation measurements at several positions in an estuary and knowledge of the river flow.

A further quantitative means of classifying estuaries has been developed by Hansen and Rattray (1966) on the basis of circulation and stratification parameters at given cross-sections of an estuary. Figure 23 shows the classification in terms of the dimensionless ratios of net surface current to mean freshwater velocity (U_s/U_f) and top to bottom salinity difference to mean cross-sectional salinity ($\delta S/S_o$) which are denoted as the circulation parameter and the stratification parameter, respectively.

In Type 1, Figure 23, the net flow is seaward at all depths and upstream salt transport is by diffusion. Type 1a has slight stratification and coincides with the laterally homogenous well-mixed estuary type. In Type 1b there is appreciable stratification. In Type 2 the flow reverses at depth and corresponds to the artially mixed estuary. Both advection and diffusion contribute to the upstream salt flux. In Type 3 the salt transfer is primarily advective: in Type 3b the lower layer is so deep that circulation does not extend to the bottom, e.g. fjords. Type 4 has more intense stratification, salt wedge type. The uppermost boundary represents conditions of fresh water outflow over a stagnant saline layer.

Based on the parameters just discussed, the classifications of the Chetco estuary are listed in Table IV.

Both Simons' and Burt and McAlister's method clearly show that the estuarine behavior is strongly dependent on the relative strength of river flow to tidal action. In general the estuary is classified as Type D in the summer while river flow is low, and Type B in the Spring and Fall while there is modest river flow and classified Type A in the Winter where river flow is high.

Classifications using the stratification number (G/J) was not applicable since no time lag in tidal height between the mouth and upstream stations was observed. The stratification number hence was not obtainable.

Field data were plotted onto the circulation and stratification diagram in Figure 23. Estuarine classification by this method shows that the Chetco estuary classification varies from season to season and from section to section as well.

Type C was not applicable to the Chetco estuary, since the river is so narrow that the Coriolis force was a negligible effect on the system. During extreme high river runoff in 1975, no salinity intrusion on the Chetco River was observed.

The opening of the new boat basin increased the tidal prism by approximately 15 percent which might provide increased saline water intrusion and increased energy brought into the estuary for mixing. However, the tidal regime changes downstream have little effect on the tidal mixing process and circulation upstream. The tidal hydrodynamic characteristics of the Chetco estuary would only be altered significantly at the mouth by the port expansion.

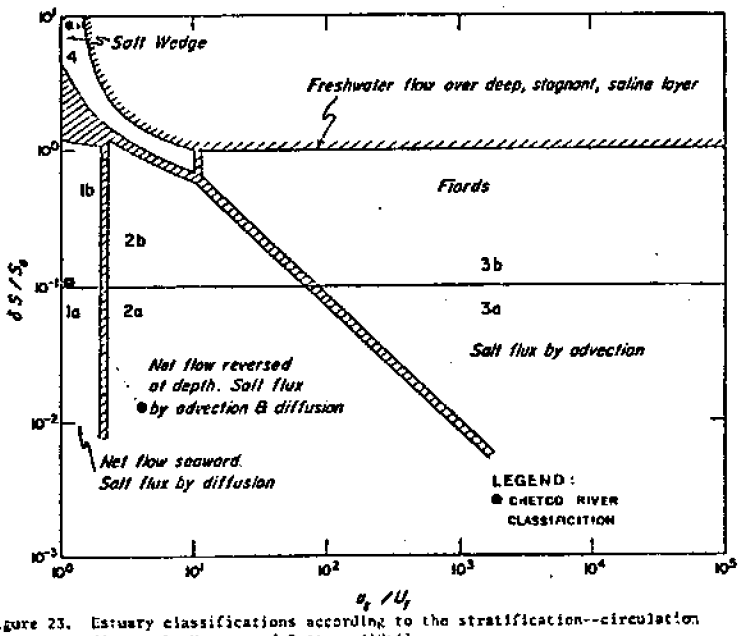

Figure 23. Estuary classifications according to the stratification--circulation diagram by Hansen and Rattray (1966).

Table IV. Chetco Estuary Classification

Date	Simmons		Burt & McAlister		Hansen & Rattray		
	Flow Ratio	Classification	Salinity Gradient	Classification	S/S_o	U_s/U_f	Classification
Feb./6 1975	18	Highly Stratified	No Salt Water Was Observed	Unclassified	-	±1	4
Jun./18 1975	0.4	Partially Mixed	±0	Well Mixed	±0	±1	1a
Sept./16 1975	0.15	Well Mixed	±0	Well Mixed	±0	±1	1a
Jan./20 1976	3.87	Highly Stratified	35	Highly Stratified	Flooding Tide 0.05	5	1b
					Ebbing Tide 0.1	1.4	2a

III. FLUSHING PREDICTIONS FOR THE BROOKINGS MARINA--ANALYTICAL MODEL APPLICATION

The flushing time of a marina is defined as the time required to renew the water accumulated within the basin during one tidal cycle by incoming seawater or river inflow. The flushing time is a parameter which describes the water exchange ability of an enclosed basin.

Tidal Prism Method:

A quick estimate of the flushing time may be calculated using the tidal prism method. Assume that in each tidal cycle, the incoming water is completely mixed with the water in the basin. Assume further that none of the water which leaves on an ebb tide will return with the next flood tide. Then, an initial concentration, Co, of pollutant in the marina at low slack tide will be diluted to a level of Ci by the volume of water which enters the marina during the next flooding tide according to the following relationship:

$$Ci = \left(\frac{V}{V+p}\right) Co$$

where V is the volume of the basin at low water level, and p is the tidal prism (volume between high water and low water).

The exchange ratio for each tidal cycle, R_E, is defined as:

$$R_E = \frac{Co-Ci}{Co} = 1 - \frac{Ci}{Co} = 1 - \frac{V}{V+p} = \frac{p}{V+p}$$

$$\therefore \text{ the flushing time} = \frac{1}{R_E} = \frac{V+p}{p}$$

For the new marina at Brookings:

$V = 2.7 \times 10^5 m^3$

$p = 7.5 \times 10^5 m^3$ for a 1.5 meter average tide.

$$\therefore \text{ flushing time} = \frac{2.7 + 1.5}{1.5} = 2.8 \text{ cycles.}$$

This time is that required to clear the basin of any given one time input of pollutant. It is known that the tidal prism method underestimates the flushing time considerably due to the incomplete mixing of basin water (Dyer, D. R., 1972).

Mixed Tank Approach:

An analytical model based on the mass balance approach for a mixed basin has been developed to examine the flushing time.

Let M be the pollutant mass in the basin at an initial time t_o, (let M_o be the pollutant concentration in the basin at time t_o, and Q_1 be the flow in or out of the basin).

If $Q_1 < 0$ (indicates net inflow)

$$\frac{dM}{dt} = 0$$

If $Q_1 \geq 0$ then $Q_1 C = -\frac{dM}{dt}$

Since $C = \frac{M}{V}$, therefore it follows that:

$$Q\frac{M}{V} = \frac{-dM}{dt} \qquad (1)$$

Integrating after separating variables

$$\frac{dM}{M} = -\frac{Q_1}{V}\,dt \qquad \frac{M_F}{M_o} = e^{-\int_{t_o}^{t_F}\frac{Q_1}{V}\,dt} \qquad (2)$$

where M_F is the pollutant mass at a final time t_F. To find an expression of Q_1 in terms of t, the flow balance between basin and open water (within a cycle), will be examined.

Assume the water depth in the basin at mean water level is ho, and let the tidal height be α. Also assume that the tides are sinusoidal. Then the water depth at any time can be expressed as:

$$h = ho + \alpha \sin(\omega t + \beta) \quad (\omega \text{ is tidal frequency} = \tfrac{2\pi}{T}) \qquad \text{-----(3)}$$

differentiating the equation above

$$\frac{dh}{dt} = \alpha\omega\cos(\omega t + \beta) \qquad (4)$$

Also let Q_o be the other new water inflow to the basin and A_s be the surface area of the basin.

The law of conservation of mass requires

$$A_s\frac{dh}{dt} = -Q_1 + Q_o \qquad (5)$$

combining Equations (4) and (5):

$$Q_o - Q_1 = A_s\,\alpha\,\omega\cos(\omega t + \beta)$$

$$\therefore Q_1 = Q_o - \alpha A_s\cos(\omega t + \beta) \qquad (6)$$

Enter equation (6) to (2) and also $V = A_s(ho+\alpha\sin(\omega t+\beta))$; then

$$\frac{M_F}{M_o} = \exp\int_{T_o}^{T_F} -\left[\frac{Q_o - \alpha\omega A_s\cos(\omega t + \beta)}{A_s(ho+\alpha\sin(\omega t + \beta))}\right] dt \qquad (7)$$

Assume that the phase angle $\beta=0$ and solve the integral part of equation (7),

$$\int_{T_o}^{T_F}\frac{Q_o - A_s\,\alpha\omega\cos\omega t}{A_s(ho+\alpha\sin(\omega t))}\,dt$$

$$= \int_{T_o}^{T_F}\frac{Q_o}{A_s(ho+\alpha\sin\omega t)}\,dt - \int_{T_o}^{T_F}\frac{A_s\,\alpha\omega\cos\omega t}{A_s(ho+\alpha\sin\omega t)}\,dt$$

-------(8)

$$= \frac{Q_o}{A_s} \frac{2}{\omega\sqrt{ho^2-a^2}}$$

$$\left[\tan^{-1}\frac{h_o\tan\frac{\omega T_F}{2}+a}{\sqrt{ho^2-a^2}} - \tan^{-1}\right.$$

$$\left.\frac{ho\tan\frac{\omega T_{O+a}}{2}}{\sqrt{ho^2-a^2}}\right] - \ln\frac{ho+a\sin\omega T_F}{ho+a\sin\omega T_O}$$

$$\pm\frac{M_F}{M_O} = \exp-\{\frac{Q_o}{A_s}\frac{2}{\omega\sqrt{ho^2-a^2}}$$

$$\left[\tan^{-1}\frac{(ho\tan\frac{\omega T_F)+a}{2}}{\sqrt{ho^2-a^2}} - \tan^{-1}\frac{ho\tan\frac{\omega T_O}{2}+a}{\sqrt{ho^2-a^2}}\right]$$

$$- \ln\frac{ho+a\sin\omega T_F}{ho+a\sin\omega T_O}\}$$

The relationship between tidal, flow and mass curves is shown in Figure 24.

Assume there is a 1.0 cms of inflow of fresh water (ground water seepage or any other source of inflow) into the boat basin at Brookings.

To evaluate $\frac{M_{F1}}{M_{01}}$ during periods of $Q_1 \geq 0$ (net outflow) at the first cycle would require

$$Q_1 = Q_o - a\omega A_s \cos\omega t \geq 0$$

$$\cos\omega t \leq \frac{Q_o}{a\omega S} = \frac{1.0}{2.5x1.4x10^{-4}x335x154} = 0.0052$$

$$\pm t_o = 1.1x10^4 \text{ sec}$$

$$t_{F1} = 3.35x10^4 \text{ sec}$$

with ho = 4.4m, a = 0.76m,

$$\omega = \frac{2\pi}{12.4x3600} = 1.4x10^{-4}$$

$$A_s = 335x154 = 5.1x10^4 \text{ m}^2$$

Entering into Equation (8)

$$\frac{M_{F1}}{M_{01}} = 0.70$$

That is, for each cycle, 0.7 of the pollutant mass remains in the basin. For a 90 percent flushing after n cycles only 10 percent of the pollutant remains.

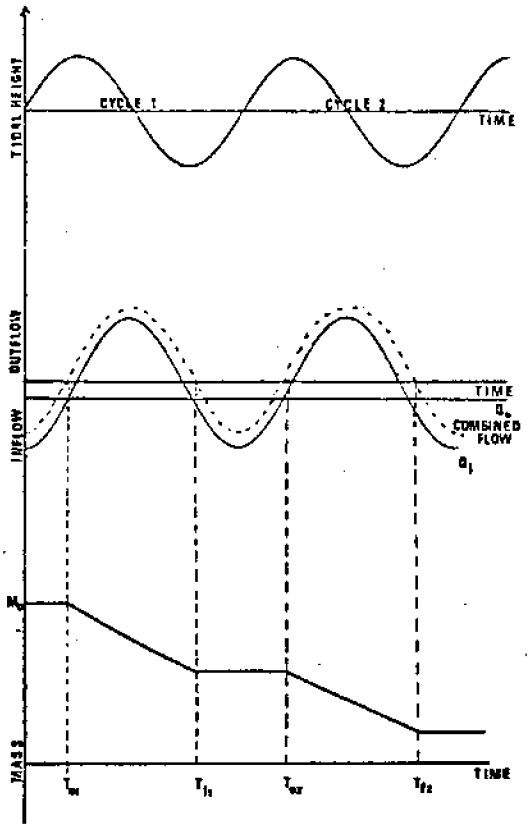

Figure 24. Tidal, flow and mass curves--Mixed Tank Approach.

$\left(\frac{M_{F1}}{M_{01}}\right)^n = (0.70)^n = 0.1$, therefore, n = 6.5 cycles

Increasing the freshwater inflow to 10 cms, then

$$t_f = 3.39x10^4 \text{ sec}$$

$$t_i = 1.08x10^4 \text{ sec}$$

during one cycle $\frac{M_{F1}}{M_{01}} = 0.66$ and it will take 5.5 cycles to dilute the pollutant to one tenth of its initial concentration.

Richey's Prediction:

A one-dimensional model has been developed by Richey (1971), for determining the excursion of a specific parcel of basin water at the end of the ebbing tide interval. The model assumes that the dominant motions in a marina may be found from a conservation of volume basis and that there is no energy loss in the entrance channel. Hence, no difference in water surface elevations between the basin and the estuary is assumed to exist.

Referring to the definition sketch in Figure 25, the conservation of mass requires that:

$$zbV - (bV + \frac{\partial}{\partial x}(bV)\,\Delta x)z = -b\Delta x \frac{dz}{dt}$$

$$\frac{d}{dx}(bV) = \frac{b}{z}\frac{dz}{dt} = \frac{bd\ln z}{dt}$$

Assume the depth is constant, i.e. $z \neq f(x)$ and integrating both sides. Since

$$V = V \qquad \text{at } x$$

$$V = 0 \qquad \text{at } x = L$$

$$\int_V^0 d(bV) = \frac{d(\ln z)}{dt}\int_x^L b\,dx$$

$$-bV\,dt = d(\ln z)\int_x^L bdx$$

$$dx = Vdt$$

$$-bdx = d(\ln z)\int_x^L bdx$$

$$-\int_{x_o}^{x}\frac{bdx}{\int_x^L bdx} = \int_{z_o}^{z} d\ln z$$

$$\ln\frac{z}{z_o} = -\ln\frac{\int_x^L bdx}{\int_{x_o}^L bdx}$$

$$\frac{z}{z_o} = \frac{\int_{x_o}^L bdx}{\int_x^L bdx}$$

$$\int_{x_o}^L bdx = \frac{z}{z_o}\left(\int_x^L bdx\right) \qquad (9)$$

For a selected final position x = L, where z = water depth at high tide and z_o = water depth at low tide, the initial position of the parcel can be found from Equation (9).

Applying the model to Brookings' new boat basin: z_o = the water depth at flooding slack, z_m = the water depth at ebb slack time, L=335 meters, b=152 meters = constant. Then Equation (9) gives

$$x_o = \left[1 - \frac{z_m}{z_o}\right] L$$

For a 1.5 meter tide, z_m=3.7 meters and z_o=5.2 meters, x_o=0.29 L. This states that a parcel of water 0.29L from the basin entrance, at high slack, could subsequently be transported to the entrance by the ebb tide. For a 2.0 meter tide, x_o=0.37 L.

Richey's model does not include the variations in velocity across the basin or in the vertical direction, as might develop in a stratified flow. All the models stated above assume that the incoming water is mixed immediately with the existing water. None of them take into account the diffusion and mixing times which actually exist.

Yearsley's Diffusion Time Prediction:

Yearsley (1974) discussed the total diffusion and mixing time of an embayment area, and expressed it as:

$$T_{diff} = \frac{\forall_{MLLW} L_{max}}{\chi A_w}$$

where $\forall_{MLLW}$ = the volume of the embayment at MLLW, in cubic meters,

L_{max} = the distance from the opening to the marina site in meters

A_w = the cross-sectional area of the opening between the embayment and open water, in square meters and

χ = the coefficient of eddy diffusity, expressed in square meters/second.

Pearson (1966) obtained a relationship between the eddy diffusity and some characteristic length scale through the examination of a large number of field measurements. Pearson's relationship is:

$$\chi = 4.64\times10^{-4} L_c^{4/3} \qquad L_c \text{ in meters}$$

Typically, L_c could be taken as the minimum dimension of the embayment. The diffusion time T can then be written as:

$$T_{diff} = \frac{\forall_{MLLW}\,\lambda}{4.64\times10^{-4} A_w L_{min}^{1/3}}$$

where $\lambda = \frac{L_{max}}{L_{min}}$

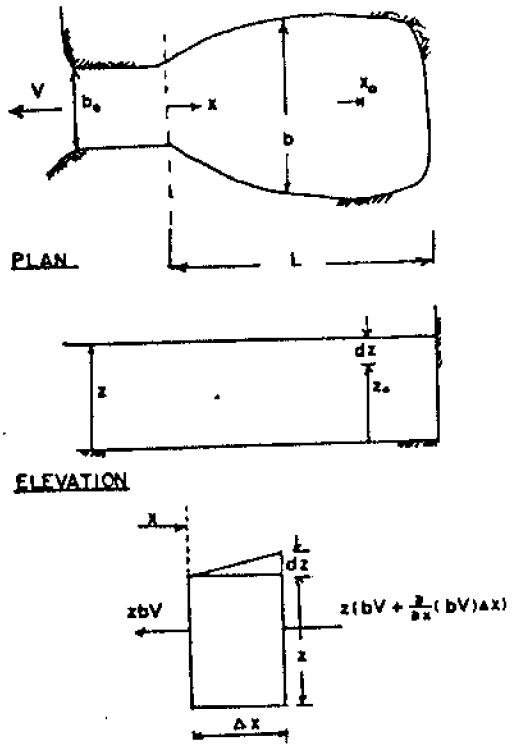

Figure 25. Definition sketch-- Richey's Prediction Method.

The required dimensions of the new boat basin at Brookings are as follows:

$$V_{MLLW} = 2.7 \times 10^5 m^3$$

$$L_{max} = 335 \text{ meters}$$

$$L_{min} = 152 \text{ meters}$$

$$A_x = 529 m^2$$

$$\lambda = \frac{L_{max}}{L_{min}} = 2.2$$

Given these dimensions, the total mixing and diffusion time is:

$$T_{diff} = \frac{V_{MLLW}^{\lambda}}{4.64 \times 10^{-4} A_w L_{min}^{1/3}}$$

$$= \frac{2.7 \times 10^5 \times 2.2}{4.64 \times 10^{-4} \times 529 \times 152^{1/3}} = 4.6 \times 10^5 \text{ sec}$$

$$= 10.34 \text{ cycles}$$

Yearsley's model provides an estimate of the overall diffusion time when there is no dispersion considered. The diffusion time of a boat basin is directly proportional to the aspect ratio and is inversely proportional to the cross-sectional area.

Besides excluding diffusion effects, the models just described also assume that the driving force of the system is the periodical rising and falling of the water surface at the mouth of the basin. Thus, ambient conditions (e.g., ambient currents, coastal processes and coastline features near the entrance, etc.) which might effect the water circulation in the basin also have been neglected. In addition, only the Yearsley's model considered the basin geometry.

There is still no dependable analytical model which combines the convection and diffusion processes for exchange predictions of marinas. The next section will be directed to determining the flushing characteristics by hydraulic modeling.

IV. FLUSHING CHARACTERISTICS OF THE BROOKINGS MARINA--PHYSICAL MODEL APPLICATION

To investigate the flushing and exchange characteristics of the new marina located at 300 meters upstream from the Chetco River mouth, a hyrdaulic scale model was constructed. The model allows the testing of engineering alternatives for improving the flushing rate if necessary. Bearing the purpose of model study in mind and with the knowledge of similarity theory, the model was designed, constructed, calibrated and verified.

The principles of hydraulic similitude of fluid motion which form the basis for the theory of models, the design of experiments, and correlation of experimental data are next reviewed.

Principle of Hydraulic Similitude:

A thorough knowledge of the principles of the mechanics of similitudes is indispensible in hydraulic research in the laboratory. Several viewpoints arise relative to the questions of similarity (ASCE, 1942). They are:

1) Geometrical Similarity: This is similarity of form. It requires the ratios of all homologous dimensions to be equal.

2) Kinematic Similarity: This is similarity of motion. It requires the ratios of the velocities of various homologous particles involved in the motion occurrences to be equal.

3) Dynamic Similarity: This is similarity masses and forces. It requires the ratios of the masses of the various homologous objects involved in the motion occurrences to be equal, and requires the ratios of the homologous forces which affect the motion of the homologous objects to be equal.

The basic concept of dynamic similarity may be stated as the requirement that two systems with geometrically similar boundaries have similar flow patterns at corresponding instants of time. Thus all forces acting on corresponding elements should have the same ratio in the two systems (Daily and Harleman, 1966).

The fluid motion of interest is the tidal propagation in an estuary. It is inherently one of the most complex types of free surface motion. The tidal flow is unsteady, non-uniform and subcritical with reversals in its direction occurring periodically. It may be non-homogenous due to salinity intrusion. The fluid is assumed to be incompressible and non-viscous. Such motion can be expressed in the form of differential equations related to momentum and mass transfer processes. Energy relations are necessary only when the energy dissipation problems due to a change in the cross-section are of interest. The general continuity and momentum equations for an unsteady, non-uniform tidal flow in vector notation are:

$$\nabla\vec{U} = 0 \qquad (10)$$

$$\frac{\partial\vec{U}}{\partial t} + (\vec{U}\cdot\nabla)\vec{U} = -\frac{1}{\rho}\nabla p + \vec{g} + \frac{\mu}{\rho}\nabla^2\vec{U} \qquad (11)$$

where $\vec{U} = U\vec{i} + V\vec{j} + W\vec{k}$, $\vec{i},\vec{j},\vec{k}$ are unit vectors in x,y,z directions

p = pressure force

g = gravitation acceleration

μ = dynamic molecular viscosity

ρ = density

A right-handed oriented coordinate system is used, with three axes x, y, z oriented such that x and y are in the horizontal plan and z is the vertical axis directed upward. The plane z=0 coincides with the mean sea level.

The condition of dynamic similarity of two flow systems can be obtained by writing Equations (10) and (11) in dimensionless forms. After choosing a characteristic length L_o and velocity U_o, all the parameters can be expressed in the following dimensionless form.

$$U^* = \frac{U}{U_o} \qquad X^* = \frac{X}{L_o} \quad Y^* = \frac{Y}{L_o} \qquad Z^* = \frac{Z}{L_o}$$

$$t^* = \frac{t}{t\ \text{characteristic}} = \frac{t}{L_o/U_o} = \frac{tL_o}{U_o}$$

Also assume that P characteristic = $U_o^2\rho$.

Where the superscript indicates the dimensionless form.

Normalizing Equation (10):

$$\frac{\partial U}{\partial X} + \frac{\partial V}{\partial y} + \frac{\partial W}{\partial z} = \frac{U_o}{L_o}\frac{\partial U^*}{\partial X^*} + \frac{U_o}{L_o}\frac{\partial V^*}{\partial y^*} + \frac{U_o}{L_o}\frac{\partial W^*}{\partial y^*} = 0$$

i.e. $$\nabla^*\vec{U}^* = 0 \qquad (12)$$

Normalizing Equation (11):

$$\frac{U_o^2}{L_o}\frac{\partial\vec{U}^*}{\partial t^*} + \frac{U_o^2}{L_o}(\vec{U}^*\cdot\nabla^*)U^* = -\frac{U_o^2\rho_o}{\rho_o L_o}\nabla^* p^* - \vec{g} + \frac{\mu U_o}{\rho L_o}\nabla^{*2}\vec{U}^* \qquad (13)$$

and dividing Equation (13) by $\frac{U_o^2}{L_o}$ results:

$$\frac{\partial\vec{U}^*}{\partial t^*} + (\vec{U}^*\cdot\nabla^*)\vec{U}^* = -\nabla^* p^* - \frac{gL_o}{U_o^2}\nabla^* h^* + \frac{\mu}{L_o U_o \rho}\nabla^{*2}U^* \qquad ---(14)$$

since $\vec{g} = -g\nabla h$, where h is taken as vertical direction (measured positively upward).

The two dimensionless coefficients appearing in Equation (14) are of particular interest in understanding dynamic similitude. The square root of the inverse of the first dimensionless group is called the Froude number. $\left(\frac{U_o}{L_o}\right)^2$ has the dimension of inertial force/unit mass.

$$F = \frac{U_o}{\sqrt{gL_o}} = \frac{|\vec{U}\cdot\nabla\vec{U}|}{|\nabla h|} = \left(\frac{\text{inertial force/mass}}{\text{gravitational force/mass}}\right)^{1/2}$$

The Froude number is an important parameter when gravity is a factor influencing the fluid motion. The inverse of the second dimensionless group, known as the Reynolds number, is important whenever viscous forces influence fluid motion.

$$R = \frac{\rho U_o L}{\mu} = \frac{U_o L_o}{\nu} \sim \frac{|\vec{U}\cdot\nabla\vec{U}|}{|\nabla\vec{U}|} = \frac{\text{inertial force/mass}}{\text{viscous force/mass}}$$

Since all of the quantities with the star superscripts are dimensionless, Equations (12) and (14) have the same solution for two geometrically similar systems, provided that the dimensionless coefficients are numerically the same for the two systems. Thus, the equality of both Reynolds numbers and Froude numbers is necessary for EXACT dynamic similitude.

Specifying the equality of Froude numbers, we have:

$$\frac{U_m}{\sqrt{g_m L_{om}}} = \frac{U_p}{\sqrt{g_p L_{op}}} \;;\; U_r = \frac{U_m}{U_p} = \sqrt{g_r L_{or}}$$

$$U_r \overset{\sim}{=} \sqrt{L_{or}} \quad (g_r = 1)$$

where L_o is a characteristic length.

From the equality of Reynolds numbers, we have:

$$U_r = \frac{\nu_r}{L_r} = \frac{\nu_r}{L_{or}} \quad \therefore L_{or} = \left(\frac{\mu_r}{\rho_r}\right)^{2/3} = \nu_r^{2/3}$$

Since both model and prototype use the same fluid (water) and the range of kinematic viscosities among the common liquids is very limited, the requirement cannot be satisfied unless the scale ratio is close to unity. Moreover, there is only one degree of freedom. That is, the choice of fluid to be used determines the length ratio.

However, the majority of hydraulic model studies of open channels, rivers and tidal estuaries, in which the fluid motions are governed by the force of gravity, fall into the category of highly turbulent, high Reynolds number flows. In these cases, the fluid friction is important but molecular viscosity effects are negligible. The questions of properly simulating the frictional effect then becomes one of considering the geometric similitude of boundary roughness rather than one of the equality of Reynolds numbers.

This is made clear by examining the terms in the dimensionless momentum equation through an order of magnitude analysis.

$$\underset{0\sim1}{\frac{\partial\vec{U}^*}{\partial t^*}} + \underset{0\sim1}{\vec{U}^*\nabla^*\vec{U}^*} = \underset{0\sim1}{-\nabla^*p^*} - \underset{0\sim1}{\frac{1}{F^2}\nabla^*h^*} + \underset{0\sim1}{\frac{1}{R}\nabla^{*2}\vec{U}^{*2}}$$

$F < 1$ for subcritical gravity flow.

$R > 10^5$ for turbulent flow. Obviously, the term $\frac{1}{R}\nabla^{*2}\vec{U}^{*2}$ is small, and therefore negligible. Hence, such hydraulic models are designed solely on the basis of Froude number similarity.

In estuarine modeling, a difficulty in non-geometric similarity arises in the form of vertical distortion. The necessity for vertical distortion arises when the area needed to be reproduced is so large that, for practical and economic reasons, the horizontal scale of the model must be made small. If the vertical scale were made the same, vertical measurements would be of such a small magnitude that accuracy would be lost. The increased water depths in the model improve the accuracy of depth and current velocity measurements, prevent undesirable capillary effects, and preserve a state of turbulence in the model.

Such procedures sacrifice the dynamic similarity of the model to a certain extent; therefore the reliability of the model predictions of certain phenomena is subject to question. It follows that the process of model verification is a vital and necessary step. That is, Froude-scaled physically distorted tidal models, if properly verified, can only simulate Froude-type phenomena such as tidal currents or gravitational circulation. Phenomena such as local currents and turbulent eddies which are not Froude-type problems are not necessarily represented in the distorted model.

The scale distortion effect on dispersion-diffusion studies has been studied by many authors, (Abraham, 1973; Fisher and Holley, 1971; Harleman, 1971; Holley and Karelso, 1973). Their results can be summarized by considering the conservation equation of conservative tracer states as:

$$\underset{(1)}{\frac{\partial C}{\partial t}} = \underset{(2)}{-U\frac{\partial C}{\partial X}} \underset{(3)}{- V\frac{\partial C}{\partial Y}} \underset{(4)}{- W\frac{\partial C}{\partial Z}} + \underset{(5)}{\frac{\partial}{\partial X} E_x \frac{\partial C}{\partial X}} + \underset{(6)}{\frac{\partial}{\partial Y} E_y \frac{\partial C}{\partial Y}} + \underset{(7)}{\frac{\partial}{\partial Z} E_z \frac{\partial C}{\partial Z}} \qquad (15)$$

where C is the concentration of the tracer and $E_{x,y,z}$ are eddy diffusities in coordinates X, Y, Z, respectively. The equation shows that the local time rate for the change of concentration is equivalent to the summation of the forces of the advective processes (terms (2), (3) and (4)) and the non-advective processes. The former are

associated with the circulation patterns, and the ...ter are associated with the eddy and turbulent mixing system. The terms (2), (3), (5), and (6) in Equation 15 indicate:

$$(E_X)_r = (E_Y)_r = (U)_r X_r = (V)_r X_r = \sqrt{Y_r}\, X_r \qquad \text{-----(16)}$$

Terms (4) and (7) show:

$$(E_Z)_r = (W)_r Y_r = Y^{5/2} X^{-1} \qquad (17)$$

Equations (16) and (17) are referred to as the required ratio for similarity.

Three combinations of characteristic parameters were developed with respect to the mechanisms associated with E_i. There are as follows:

$$E = KU^*H \qquad (18)$$

$$E = KUH \qquad (19)$$

$$E = KUL \qquad (20)$$

where U* represents the shear velocity $=(RgS)^{1/2}$

K is a proportionately constant,
L is the horizontal characteristic length,
H is the vertical characteristic length scale, and
σ is shear stress.

It is apparent that there is a direct conflict between the similitude requirement for the ratios of eddy coefficients as expressed in Equations (16) and (17) and the ratios of eddy coefficients when the fluid mechanisms associated with diffusion are considered, as expressed by Equations (18), (19) and (20).

A physical explanation is that the magnitude of the eddy coefficients is governed by the nonuniformity of the velocity. Figure 26 points out that a distorted model changes both the vertical and the transverse velocity gradient. An even greater change in the velocity distribution results from the use of artificial roughness elements.

Table V is the comparison of the diffusion coefficient between required and actual values, referring to the three expressions stated previously. The comparisons are made both for the distorted and undistorted models. It points out that the error depends on the scale distortion ratio $(\frac{X_r}{Y_r})$ and the processes governing the dis...sion.

Table V. Comparison of Diffusion Coefficients of Actual and Required Values in Undistorted and Distorted Models.

Model Type	$E_{X,Y}$ Required	E_Z Required	Actual/Required Based on					
			KU*H		KUH		KUL	
			$E_{X,Y}$	E_Z	$E_{X,Y}$	E_Z	$E_{X,Y}$	E_Z
Undistorted	$X_r^{3/2}$	$X_r^{3/2}$	1	1	1	1	1	1
Distorted	$X_r Y_r^{1/2}$	$X_r^{-1} Y_r^{5/2}$	$(\frac{X_r}{Y_r})^{-3/2}$	$(\frac{X_r}{Y_r})^{1/2}$	$(\frac{X_r}{Y_r})^{-1}$	$(\frac{X_r}{Y_r})$	1	$(\frac{X_r}{Y_r})^2$

check
R = Hydraulic Radius ≈ H
$U^* = (gRS)^{1/2}$

ACTUAL CROSS SECTION

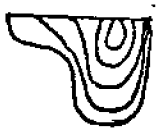

VERTICALLY DISTORTED CROSS SECTION

Figure 26. Comparison of velocity contours in prototype and distorted model.

Due to the above reasoning, a direct simulation of the distribution of substances in distorted physical models is unpractical. The results of such a model study should not be relied upon too heavily for application at specific locations, except for gaining qualitative information.

In the following model study, the primary interest is in the movement of water in and out of the boat basin at the Port of Brookings. In other words, the main concern is how long it will take to flush away the water accumulated in the basin during one tidal cycle, rather than the exact concentration distribution of pollutant in the basin. In the model, a fluorescent dye was used to trace a mass of the water's movement. Neither diffusion, dispersion processes, nor substance distribution were of interest. Reduced-scale physical models with vertical distortion, after careful verification, have proven to be very useful in studying circulation and water quality problems (Simmon, 1971; Carstens, 1972; Nece and Richey, 1975). An assumption was made that any pollutant which was dumped in the water would become well mixed with the water particles and would follow the motion of the water particles.

Model Design:

The behavior of a basin in terms of circulation and water exchange is dependent upon many factors, but depends principally upon the tidal variation, fresh water inflow and basin geometry. Hence, it is desirable that the ocean tide and river inflow be accurately reproduced. Phenomena not modeled hydraulically include: wind waves, longshore currents, oceanic currents, wind-induced currents and stratification caused by salinity variation. Floating piers and moored boats have had little effect on gross current patterns as seen in other similar studies (Nece and Richey, 1972), so they were not reproduced in the Port of Brookings model.

In a river in which the tide gradually dies out in the upstream direction, the uppermost section was chosen far enough upstream so that the vertical tidal motion is negligible and the fresh water discharge is equal to the river flow. The model layout is shown in Figure 27. A photograph of the model is shown in Figure 28. The uppermost one mile of the river has been bent slightly in order to fit the available space.

The model has a horizontal scale of 1:300 and a vertical scale of 1:30. Scale selection was based on such factors as:

a) Duplication of geometric, kinematic and dynamic force ratio (see previous discussion).
b) The depth of water required in the model to prevent excessive bottom friction effects. (This requires the Reynolds number in the model to be larger than 10^3 (Carstens, 1973).
c) Space available and cost of construction.
d) Efficiency of model operation.
e) Capabilities of reproduction and measuring equipment.

After selection of the model scale, the model was designed and operated accoring to Froude's Model law, which resulted in the following model to prototype scales:

Characteristic	Dimension[1]	Model to Prototype Scale Relation
Horizontal Length (X)	X_r	1 : 300
Vertical Length (Y)	Y_r	1 : 30
Surface Area (A_s)	Y_r^2	1 : 90,000
Cross-sectional Area (A_c)	$X_r Y_r$	1 : 9,000
Time (T)	$X_r Y_r^{-1/2}$	1 : 54.8
Velocity (V)	$Y_r^{1/2}$	1 : 5.48
Discharge (Q)	$L_r Y_r^{3/2}$	1 : 49,300
Diffusion Coefficient (E)[2](K&H*)	$Y_r^2 X_r^{-1/2}$	1 : 52.0
Roughness (n)	$Y^{2/3} X^{-1/2}$	1 : 0.56

Selection of Test Conditions:

The purpose of the model study was to find the memorizational potential of the boat basins. The memory of a water body, described by the parameter denoted as flushing time or resident time, depends on the basin geometry and on the amount of input energy provided by tidal action and fresh water inflow. Once the geometry is fixed, the memory is only a function of input energy. With less energy input, the memory becomes longer, and vice versa. Due to the wide variation of tides and river flows in the prototype, it is impossible and impractical to simulate each possible set of conditions. Hence, some averaged sets of conditions were selected for the hydraulic model tests.

These conditions were:

Case 1) An average tide with a 1.5 meter (5 feet) range and a low river inflow of 5.8 m^3/sec (200 cfs).
Case 2) An average tide with a 1.5 meter (5 feet) tidal range and an average high river runoff of 255 m^3/sec (9000 cfs).
Case 3) A large tide with a range of 2.1 meters (7.0 feet) and a low river runoff of 5.8 m^3/sec (200 cfs).
Case 4) A large tide with a range of 2.1 meters (7.0 feet) and a high river runoff of 255 m^3/sec (9000 cfs).

The mean tidal level for the fours cases was selected as 1.13 meters (3.7 feet) above local mean lower low water level.

Description of Model and Appurtenances:

The Chetco estuary hydraulic model was built and contained within a cinder brick tank which was sealed with a natural rubber liner. Sand was compacted as a filler. Bathymetric data were reduced to templates according to proper scales, and then firmly fixed in position. Actual modeling of the model surface then followed by molding the last 2 centimeters of surface with cement

CHETCO RIVER HYDRAULIC MODEL

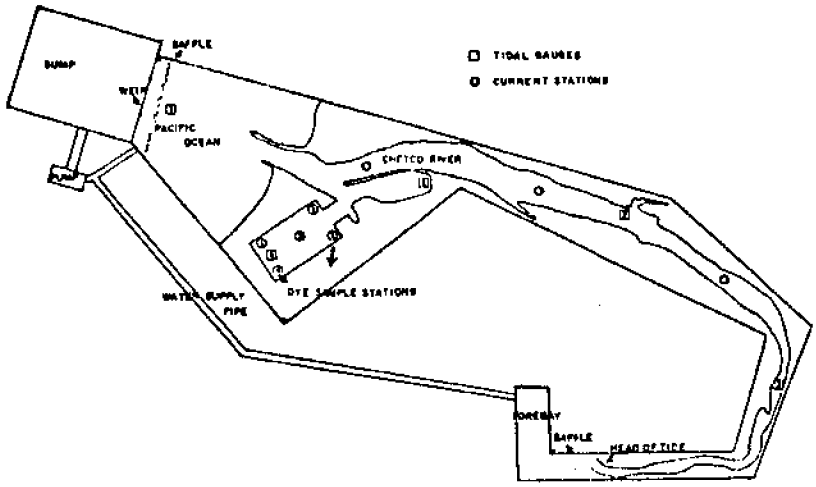

Figure 27. Chetco River hydraulic model layout

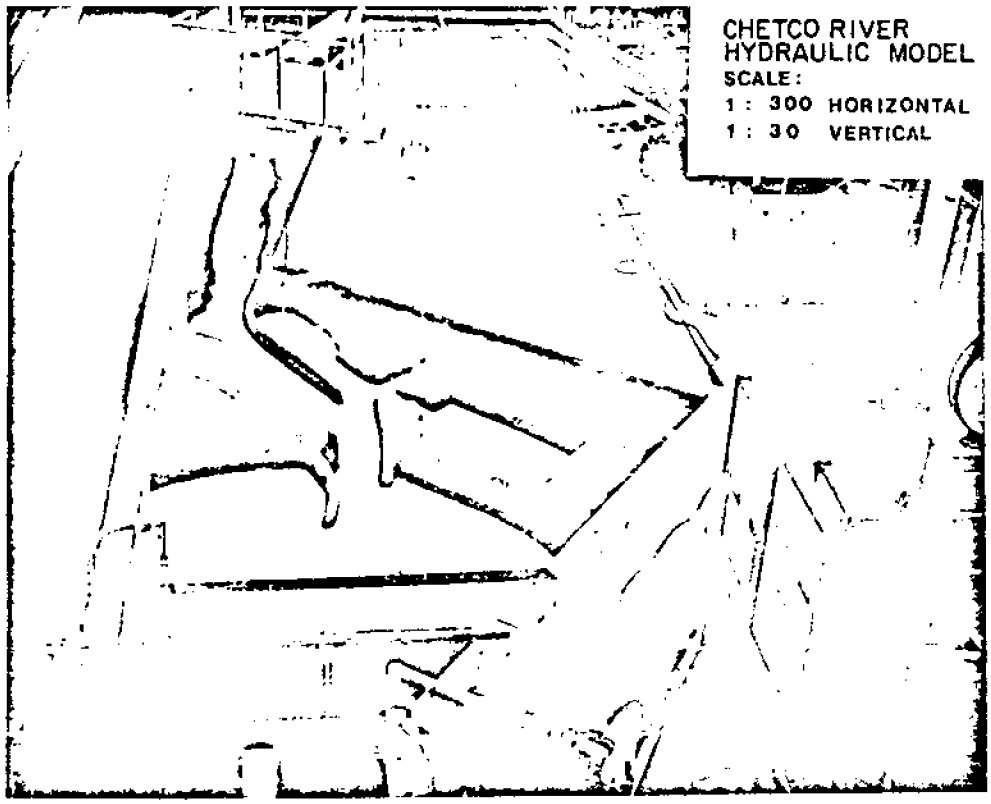

Figure 28. Photograph of the Chetco River hydraulic model, scale of 1:300 horizontally and 1:30 vertically.

mortar. While the cement curod, a water sealer was applied on the surface. Finally the area under mean lower low water (MLLW) was painted white to improve visualization of flow, to enhance photographic records, and to prevent the dye used for tracing water masses from being absorbed by the surface of the model.

Tides were reproduced in the model by a tide generating system. The tidal generator was a variable-elevation waste weir, driven by a small motor through appropriate gear reducers. It had an adjustable cam to obtain harmonic motion, and was fed by a constant-rate water supply. It provided semi-diurnal tides with a range varying from 3.5 centimeters to 7.6 centimeters (1.0 ∿ 2.25 meters in the prototype). A 1.5 meter range tide generated in the hydraulic model is shown in Figure 29. A water supply sump stored and provided water required for inflow and outflow. River flow was pumped from the same sump. A rotary flow meter and a gate valve were used to control the simulated river flow rate.

Water surface measurements were made by two sonic profile transducers (Model 86) and two Wesmar level monitors (Model SLM 9). Both measurements systems operate on the basis of measuring the propogation time of a sonic pulse which travels to the water surface and returns. The time samples are converted into a voltage proportional to the distance between sensing head and water surface. Refer to Figure 27 for the locations of tidal stations.

Current velocity measurements were made in the model with a miniature current flowmeter (Novar Streamflo Probe 403). The diameter of the miniature measuring head, with a cage, is approximately 1.5 centimeters The measuring head consists of a five bladed rotor mounted on a hard stainless steel spindle. The spindle terminates in fine burnished conical pivots, which run in jewels mounted in an open frame. Frictional torque is thus extremely low, and resulting in a linear output over a wide range of flow velocities from 2.5 to 150 centimeters per second (0.14 m/sec ∿ 8.2 m/sec in prototype).

In areas where currents were weak, either dye or miniature drogues were used to determine the current velocity.

In order to measure the relative fluorescence of the dye tracer, a Turner Model III Fluorometer was used. The fluorometer is basically an optical bridge that detects the difference between light emitted by the sample and that emitted from a rear light path. The fluorometer was calibrated before each test.

Hydraulic Model Calibration:

Calibration of a model is the most important step in assuring reliable predictive abilities, for the model must first show its ability to reproduce past events. Theoretically, the calibration can only be carried out with known prototype conditions. However, the reproduction of the prototype tides can be complicated. Instead of following the conventional calibration method of directly using prototype data, the water surface elevations and current information produced by the numerical model with semi-diurnal input tides were used to calibrate the physical model.

Based on this information, the Chetco River hydraulic model was adjusted by adding metal screens until the water surface elevations correspond to those of the prototype and the cross-sectional average velocities of the two systems were approximately equal. The calibration was carried out both in high and low river flows (255 m^3/sec river inflow, 2.1 meters tide and 5.7 m^3/sec, 1.5 meter tide). A comparison of water surface elevations between model and prototype at Station 3 for high river runoff is shown in Figure 29. A comparison of water surface elevations at Stations 3 and 5 is also shown in Figure 29. The cross-sectional averaged current velocites for Stations 2 and 4, for physical and numerical models, are compared in Figure 30 and 31 for high river flow and low river flow conditions, respectively. The water surface elevations between physical and numerical models show satisfactory agreement. The comparisons of average velocities show some disagreement in magnitude but the shapes of the curves are well matched. Since there were some uncertainties in velocity measurements and flow calculations, the discrepancy is considered to be acceptable.

Tests and Results:

The following tests were designed to examine the flushing characteristics of the Port of Brookings' new marina.

Flushing Tests:

To determine the rate of water exchange, Rhodamine WT dye was used as a tracer. In a series of tests, it was injected into different parts of the basin, and its dilution was observed. Rhodamine WT was selected since it has a relatively low degradation and suffers only small losses by absorption. The relative fluorescence of the sample water containing dye gave an index of the dye concentration.

The flushing test procedure followed was:

1) A barrier was placed to separate the water in the boat basin from the ambient stream circulating water at high tide.
2) Dye was mixed in the basin; standard samples were taken for background control; the initial dye concentration was arbitrarily assigned a 100 percent ratio denoted as C_o.
3) The dividing barrier was removed; the tide generation was continued or restarted.
4) Dye samples were selectively obtained from surface and bottom at the stations shown in Figure 27, following each high slack.

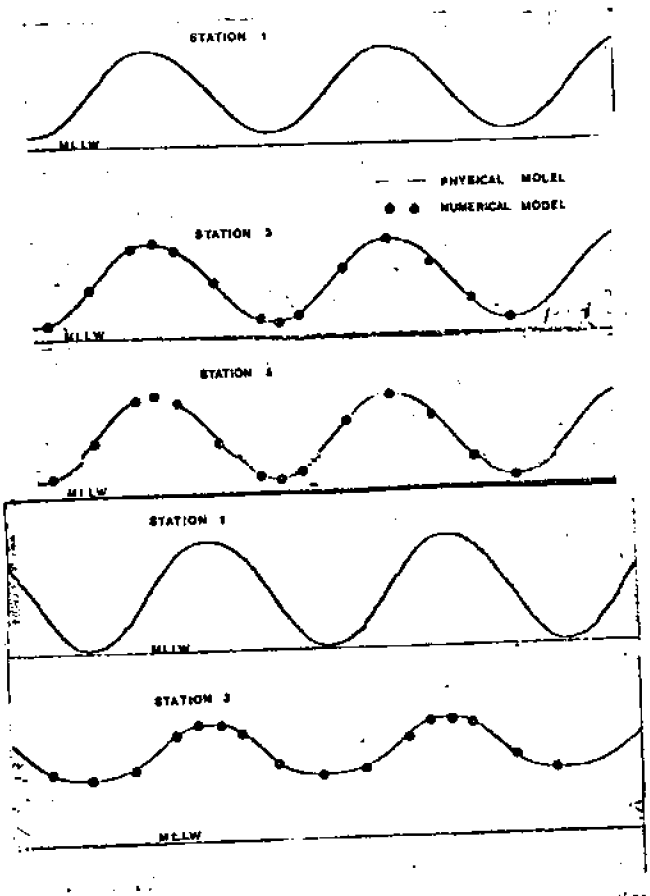

Figure 29. Comparisons of the water surface elevations between numerical and physical model predictions at station 3 and 5 for a 1.5 meter tide with a 5.8 m^3/sec. river flow and atstation 3 for a 2.1 meter tide with a 255 m^3/sec. river inflow.

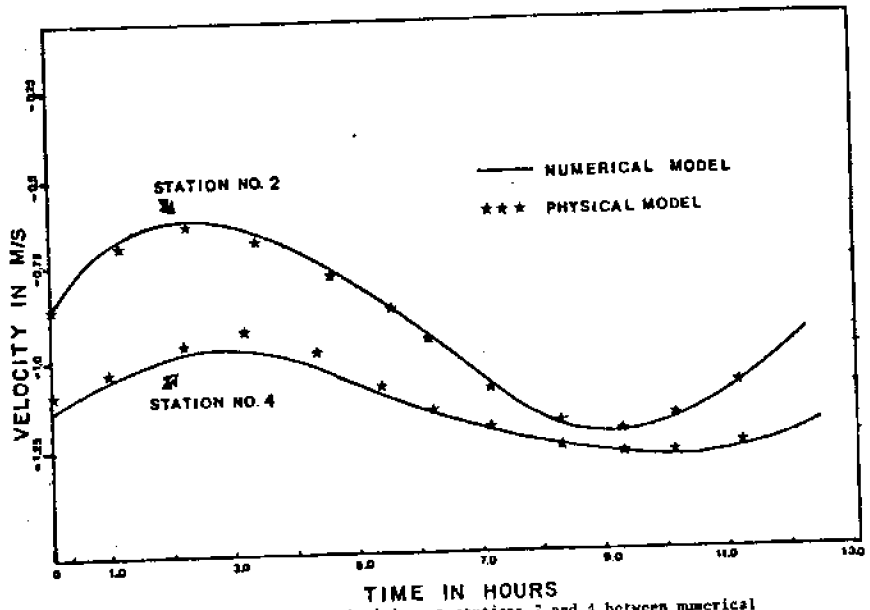

Figure 30. Comparisons of average velocities at stations 2 and 4 between numerical model predicted value and physical model measurements for a 2.1 meter tide with a 255 m^3/sec. river flow.

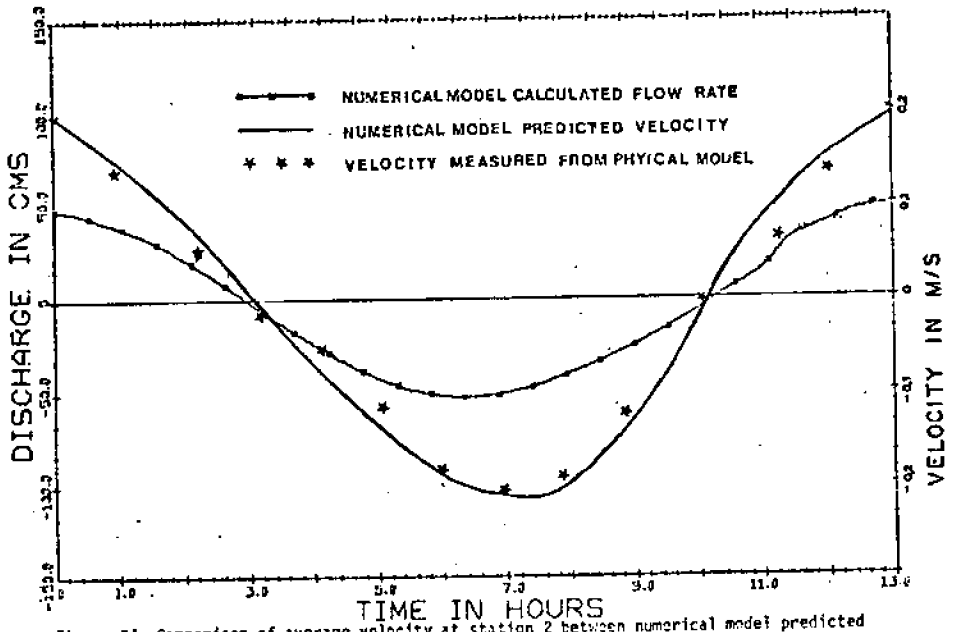

Figure 31. Comparison of average velocity at station 2 between numerical model predicted value and physical model measurement for a 1.5 meter tide and with 5.8 CMS river inflow.

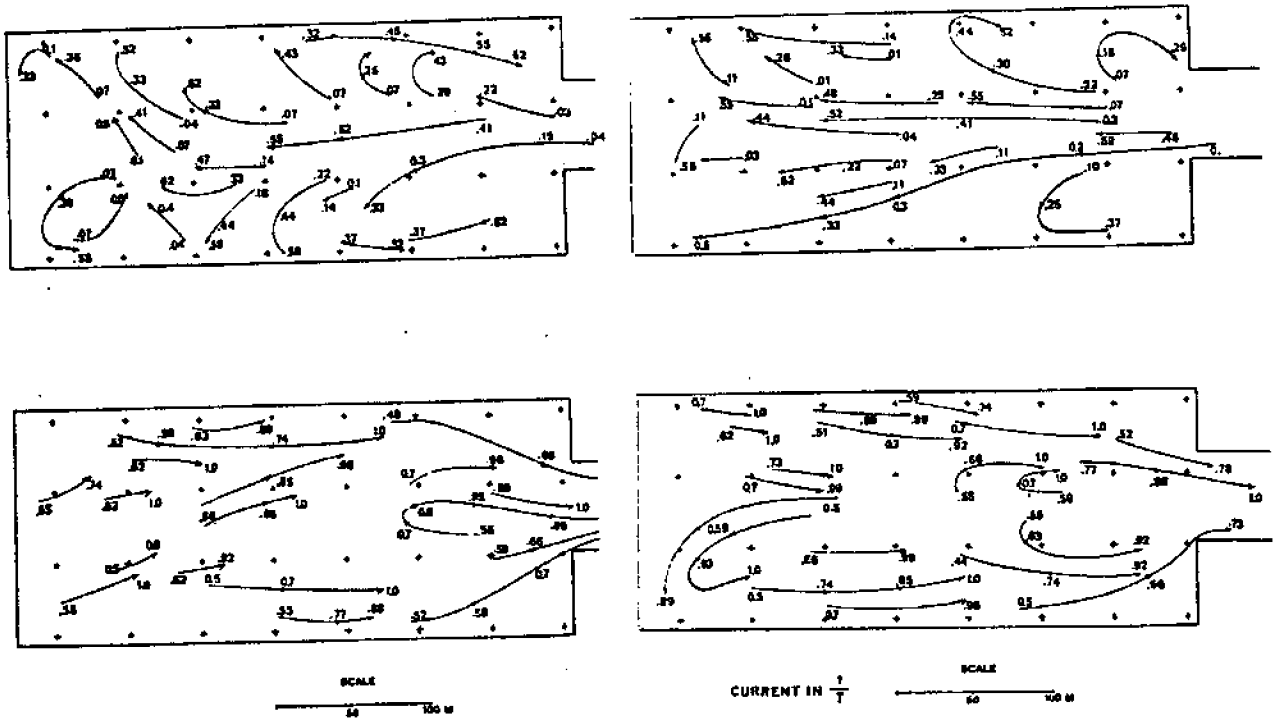

Figure 32. Miniature-float pathlines in the new boat basin, Port of Brookings. Simulating a 1.5 meter tide and 5.8 m³/sec. ambient river runoff.

Figure 33. Miniature-float pathlines in the new boat basin, Port of Brookings, Simulating a 1.5 meter tide and 255 m³/sec. ambient river runoff.

5) After three or four tidal cycles, depending on how well the basin flushed, the basin was again closed at high slack.
6) The water in the basin was stirred or remixed; final dye samples were taken; the relative concentration of the remaining dye C_n was determined.
7) A 90 percent flushing time was defined as the time required to move 90 percent of the water accumulated in the basin within one tidal cycle.

Denoting the average retention coefficient per tidal cycle as R, then:

$$\frac{C_1}{C_o} = R, \frac{C_2}{C_1} = R, \ldots\ldots\ldots \frac{C_n}{C_{n-1}} = R.$$

$$\frac{C_n}{C_o} = R^n \quad \text{so} \quad R\left(\frac{C_n}{C_o}\right)^{\frac{1}{n}}$$

The number of cycles required to flush 90 percent of the water from the basin is:

$$0.1 = \left[\left(\frac{C_n}{C_o}\right)^{\frac{1}{n}}\right]^m$$

Thus the 90 percent flushing time is:

$$m = \frac{-1}{\frac{1}{n}\log\left(\frac{C_n}{C_o}\right)}$$

The purposes of the flushing test were to determine the gross water exchange rate of Brookings new boat basin, and to reveal potential stagnant regions inside the boat basin.

Circulation Pattern Study:

Miniature drogues were made for tracing surface and subsurface water movements. Time-lapse photographs of the drogues' movements were made for each 1/8 tidal period. The time-lapse for each photograph was 25-30 seconds, which is equivalent to 23-27 minutes in the prototype. The traces left by the drogues represent the instantaneous stream lines, and reveal surface current patterns.

Surface and subsurface drogues were traced over time and space on a plexiglass sheet superposed on the boat basin planform. The pathlines represent the surface and subsurface water movements.

Test Results:

Flushing tests were done for each of the selected cases; the experimental results are presented in Table VI. A higher tidal range as well as high ambient river currents were found to increase the basins flushing ability. The 90 percent flushing time varied from four to eight cycles, depending on the tidal range, ambient river flow and other meteorological conditions.

Typical float pathlines are shown in Figures 32 and 33 for a 1.5 meter tide with river runoffs of 5.8 m^3/sec. and 255 m^3/sec. respectively. Also, Figure 38 shows the water particle movements for 1.8 meter tide with an 80 m^3/sec river runoff. No difference between surface and subsurface float paths were observed. The current was expressed in t/T, where t was the time elapsed after low slack and T was the tidal period. The crosses are spaced 45.7 meters apart. From examination of these curves during the ebbing period, it was found that the only water particles which could escape from the basin were those located less than a distance of one third of the basin's length from the entrance. This result corresponds to Richey's prediction (Chapter III).

Figures 34 a-i show the instantaneous flow circulation patterns for a 1.5 meter tide and 5.8 m^3/sec. river runoff, compared with Figure 35 a-h which represents the situation with a river runoff of 255 m^3/sec. The camera's shutter opening time was 25 seconds in Figure 34 and 30 seconds in Figure 35. Note that the clock in the photo gives the relative time of the tidal phase and also indicates the length of time the camera's shutter was open.

An examination of Figures 32 through 35 shows that circulation cells exist in the basin. For the same range of incoming tides, the size and number of cells depends on the strength of the incoming currents.

Hydraulic Model Verification:

Model verification is a process by which a hydraulic model is tested to determine its ability to reproduce certain phenomena which have been observed in the prototype. The need for verification is imperative because flow processes involving mixing, diffusion, dispersion and therefore flushing are influenced by geometric distortion of the model's cross-section and its effect on the velocity distribution. Therefore, following the opening of the new boat basin, a field trip was conducted for the purpose of evaluating the flushing ability of the new boat basin at Brookings and for comparison with the hydraulic model results. A dye flushing study was performed in the field. Rhodamine WT dye was mixed into the basin at high slack tide. Control samples were taken immediately after the release. Surface and bottom samples were subsequently taken from the stations noted on Figure 36 at the first, third and fifth high slack after the dye mixing. The field trip was scheduled so that the tidal ranges during the field experimental period were nearly the same. The average tidal range of the six cycles was 1.83 meters and the average river runoff then was approximately 80 m^3/sec.

The 90 percent flushing time obtained from the 1976 field study was 6.9 cycles. A test with the same tide and river runoff conditions was run in the hydraulic model. Dye samples were also taken from the corresponding stations where samples were taken in the field. The 90 percent

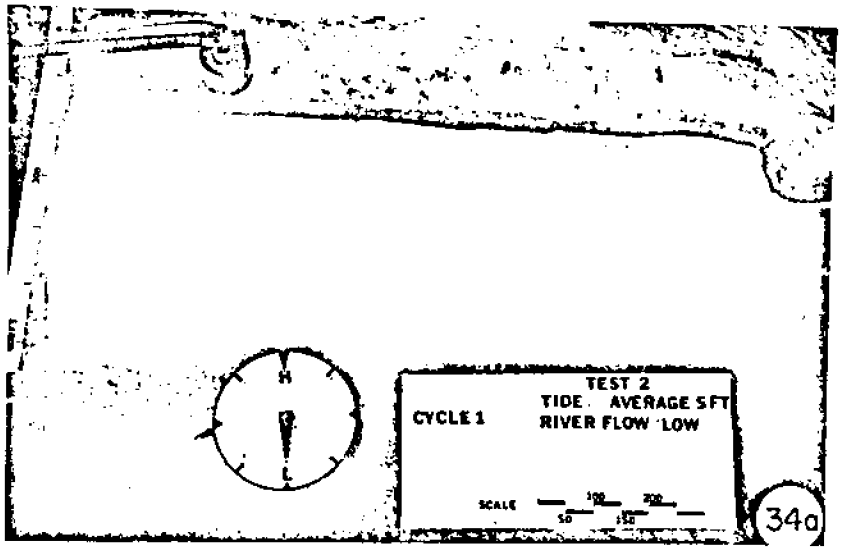

34a

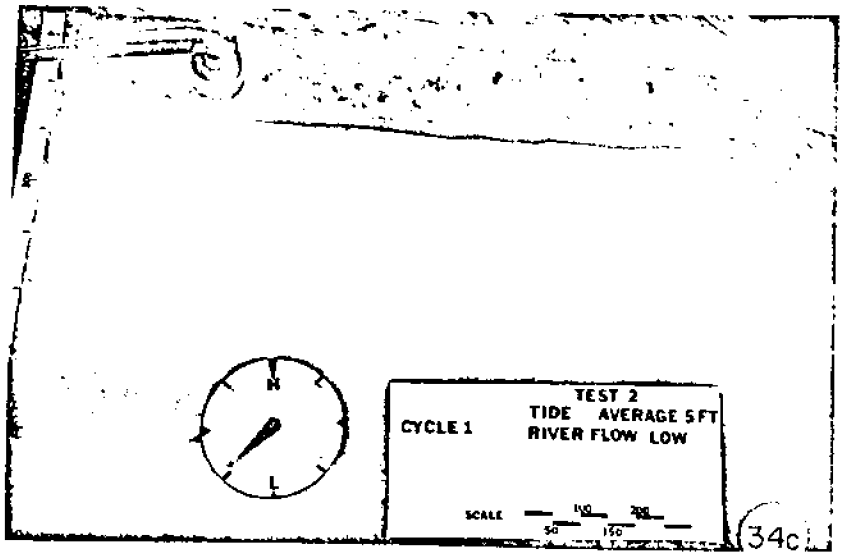

34c

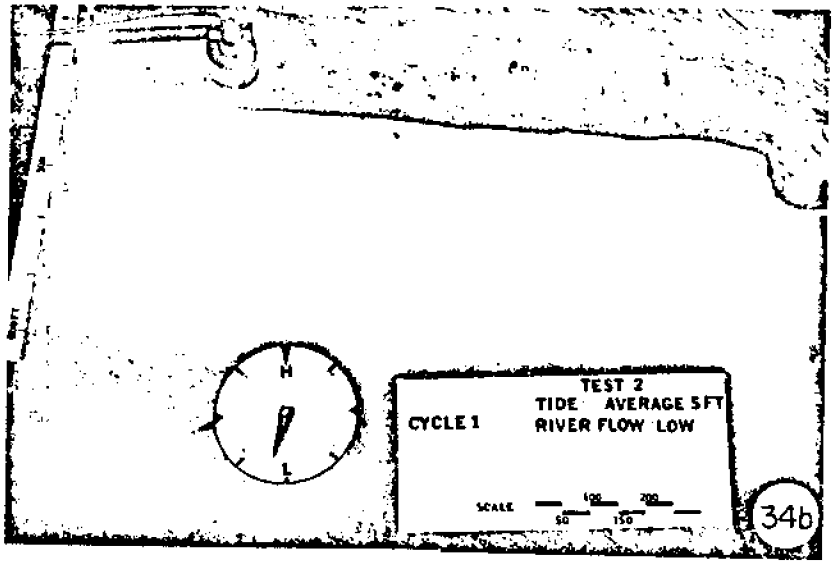

34b

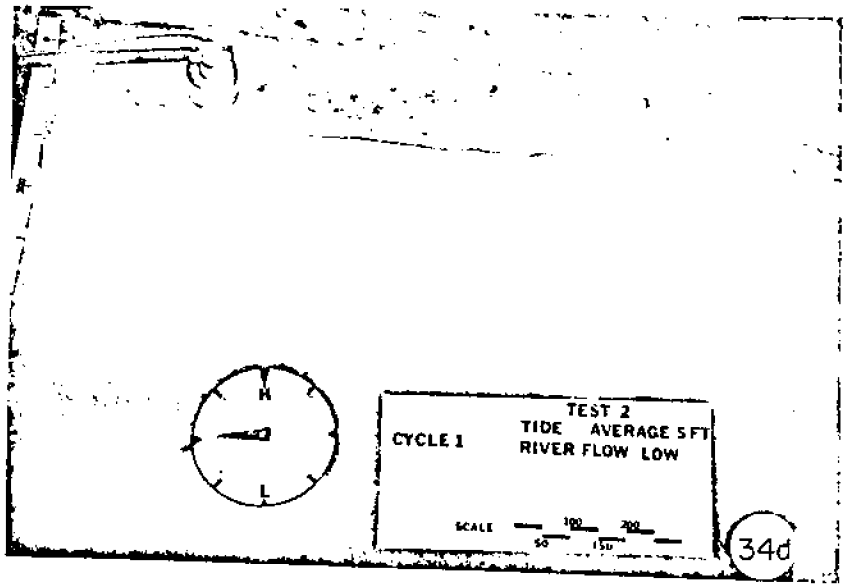

34d

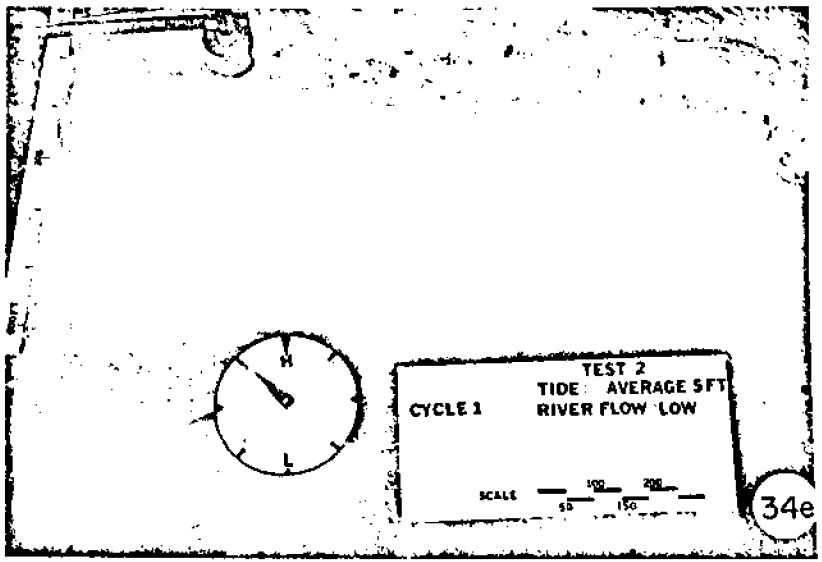
H
L
TEST 2
TIDE AVERAGE 5 FT
CYCLE 1
RIVER FLOW LOW
SCALE
34e

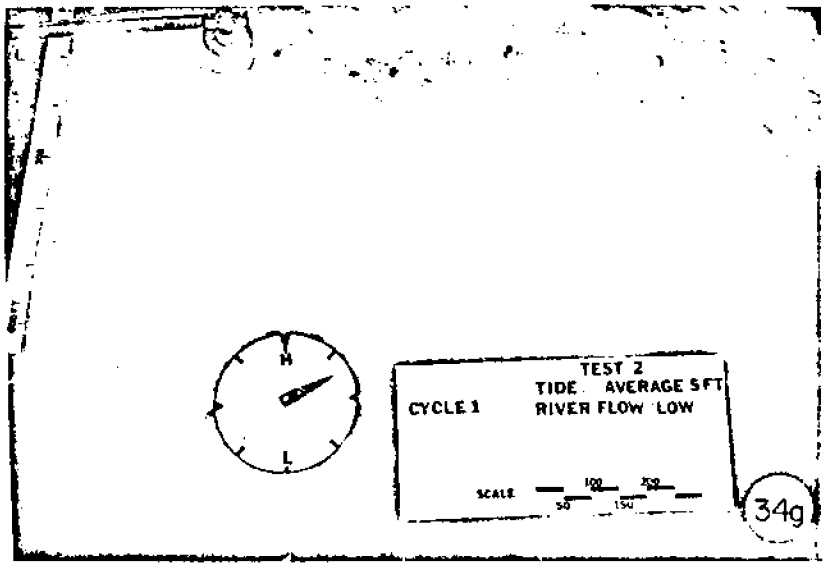
H
L
TEST 2
TIDE AVERAGE 5 FT
CYCLE 1
RIVER FLOW LOW
SCALE
34g

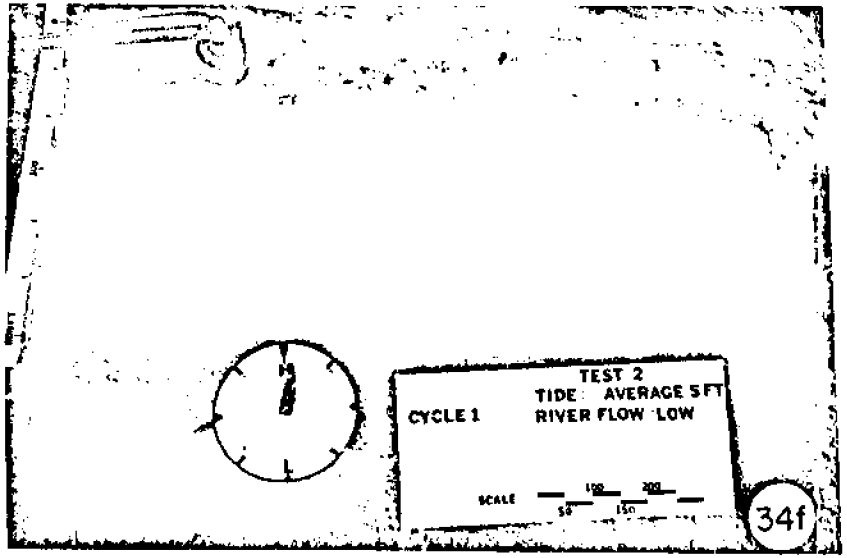
H
L
TEST 2
TIDE AVERAGE 5 FT
CYCLE 1
RIVER FLOW LOW
SCALE
34f

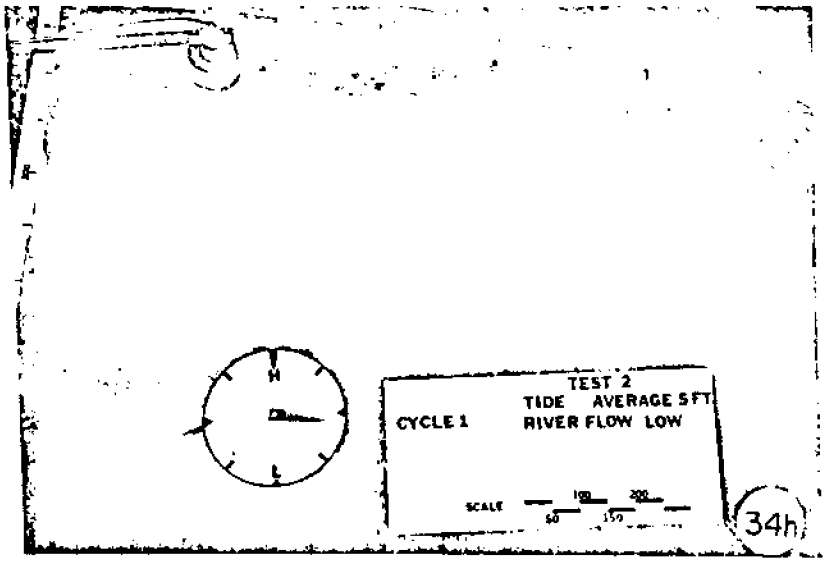
H
L
TEST 2
TIDE AVERAGE 5 FT
CYCLE 1
RIVER FLOW LOW
SCALE
34h

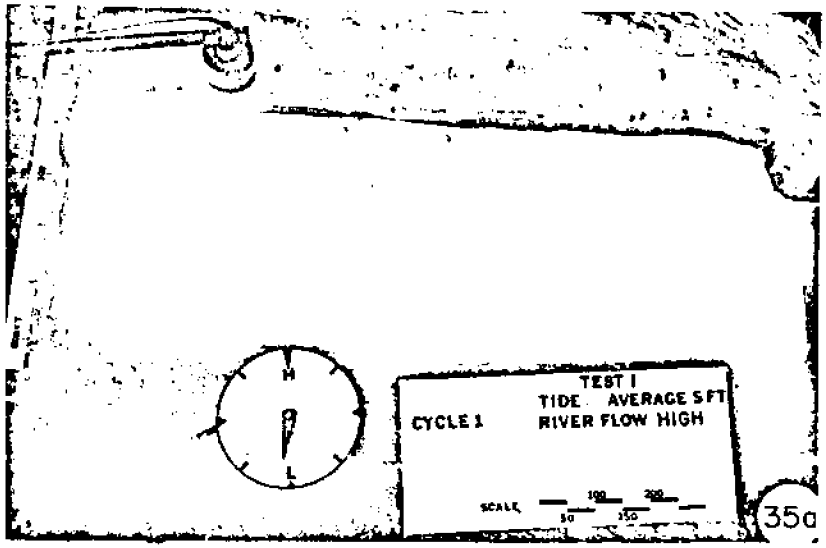
H
L
TEST I
TIDE AVERAGE SFT
CYCLE 1
RIVER FLOW HIGH
SCALE
35a

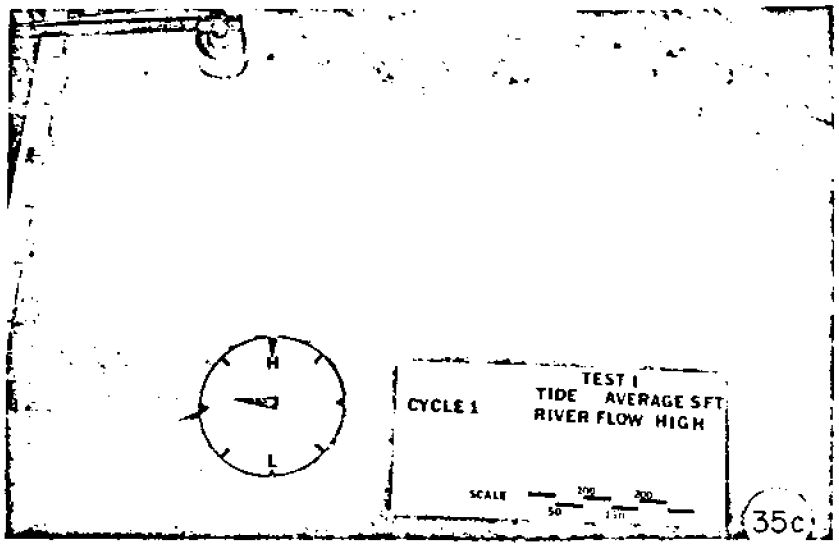
H
L
TEST I
TIDE AVERAGE SFT
CYCLE 1
RIVER FLOW HIGH
SCALE
35c

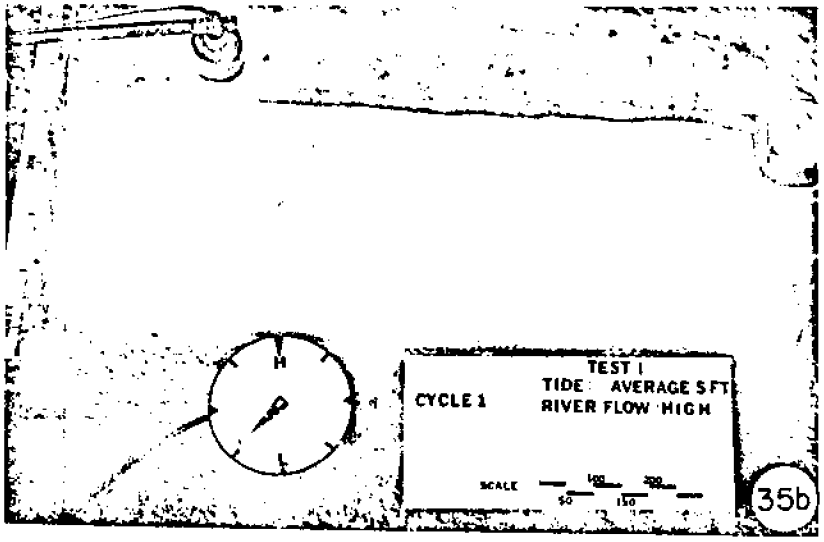
H
L
TEST I
TIDE AVERAGE SFT
CYCLE 1
RIVER FLOW HIGH
SCALE
35b

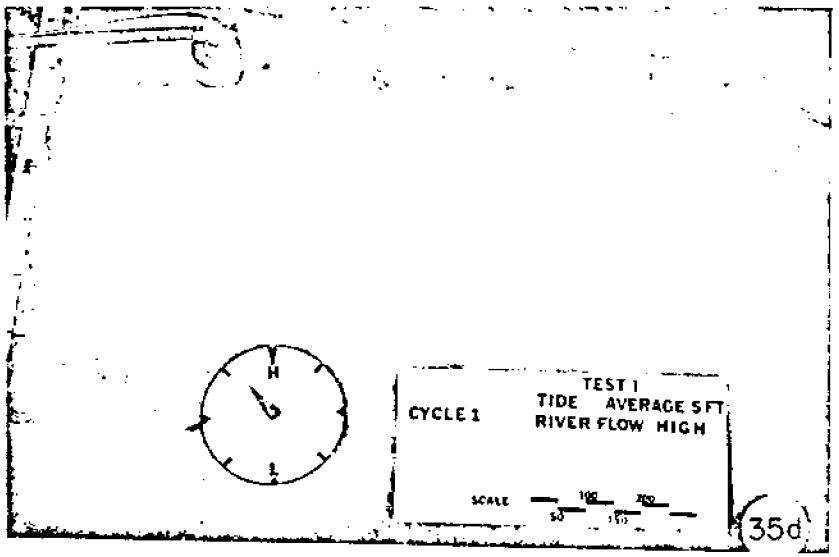
H
L
TEST I
TIDE AVERAGE SFT
CYCLE 1
RIVER FLOW HIGH
SCALE
35d

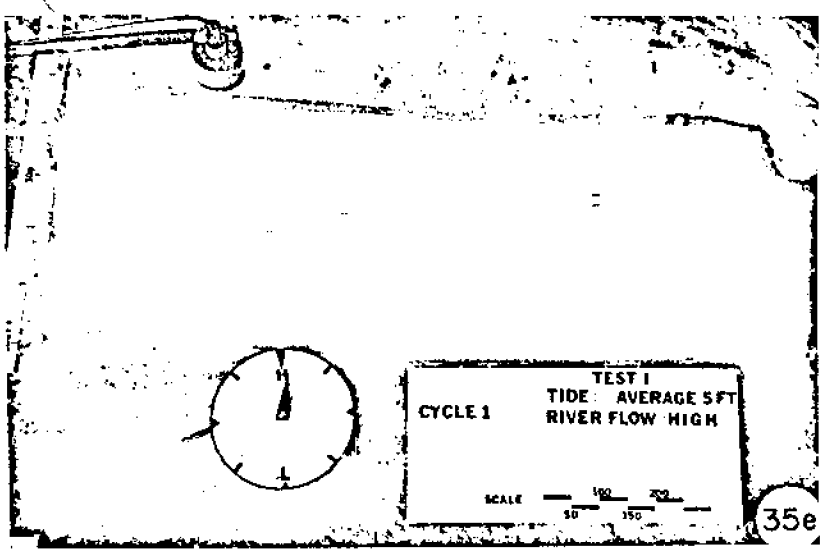
H
L
TEST I
CYCLE 1
TIDE AVERAGE 5FT
RIVER FLOW HIGH
SCALE
35e

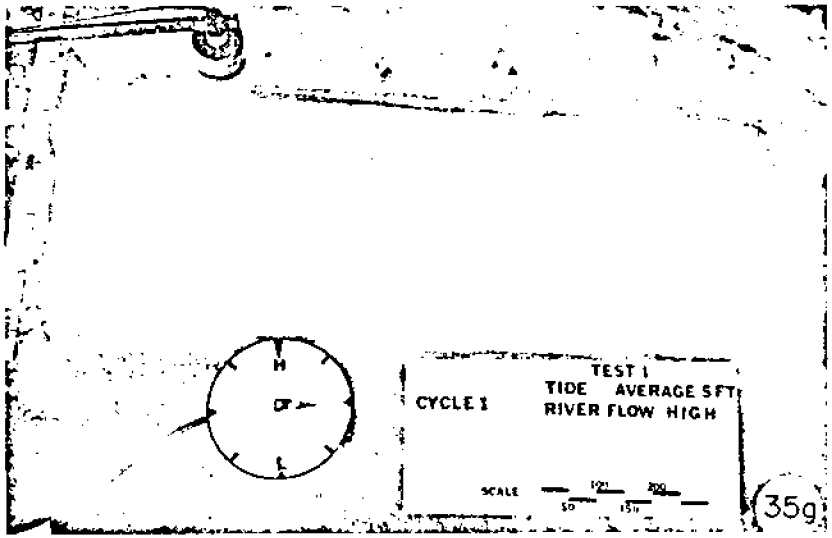
H
L
TEST I
CYCLE 1
TIDE AVERAGE 5FT
RIVER FLOW HIGH
SCALE
35g

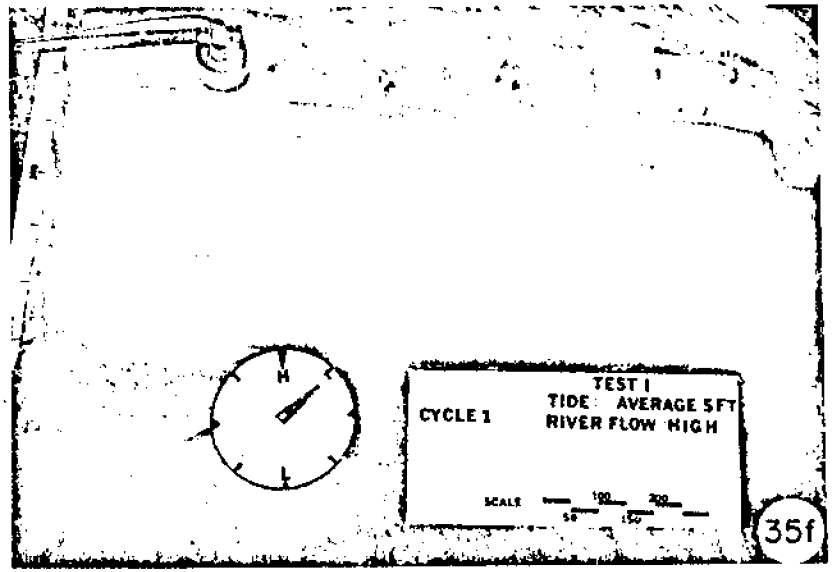
H
L
TEST I
CYCLE 1
TIDE AVERAGE 5FT
RIVER FLOW HIGH
SCALE
35f

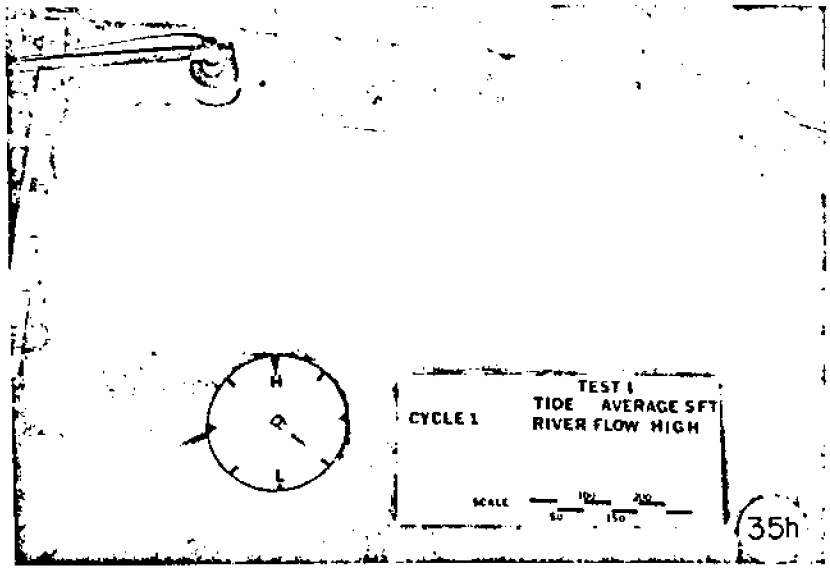
H
L
TEST I
CYCLE 1
TIDE AVERAGE 5FT
RIVER FLOW HIGH
SCALE
35h

Table VI. Summary of Physical Model Prediction Flushing Times for Select Test Cases

Test Condition			Result
Case	Tidal Height (m)	River Inflow (CMS)	90% Flushing Time in tidal cycles
I	1.5	5.8	7.6
II	1.5	255.0	5.7
III	2.1	5.8	6.3
IV	2.1	255.0	4.3

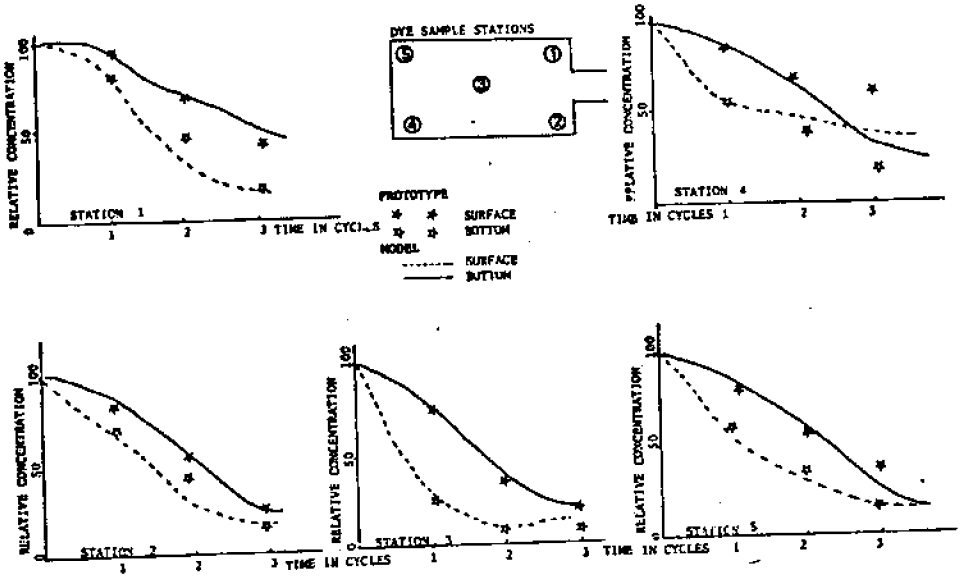

Figure 56. Comparison of dye concentrations taken from the field and the hydraulic model

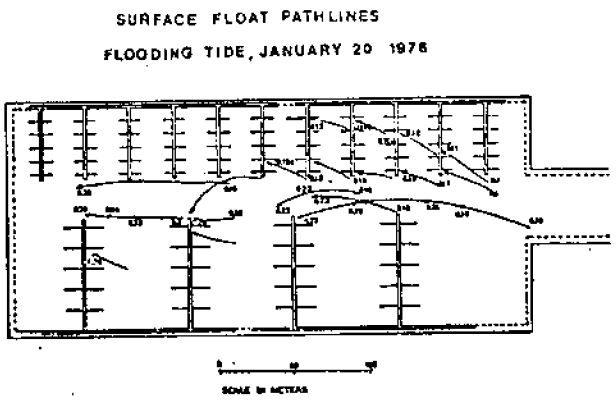

Figure 37. Drogue pathlines, observed on January 20 1976.

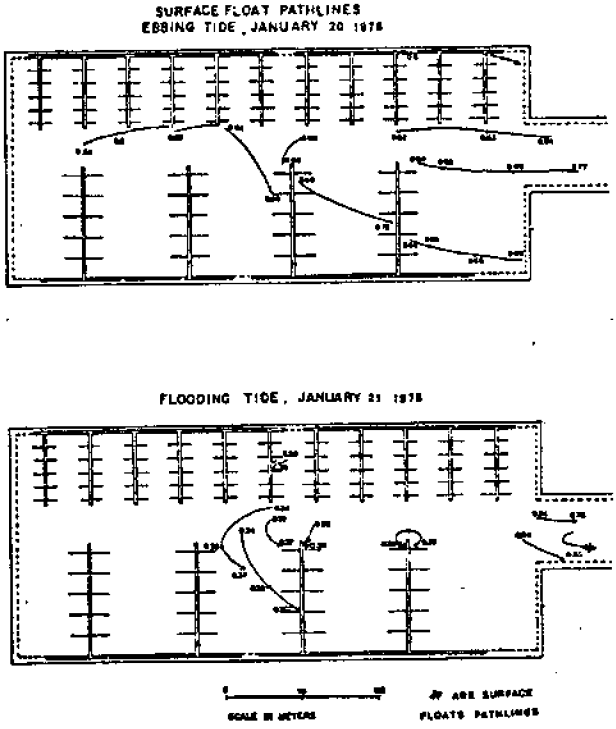

Figure 38. Drogue pathlines, observed on January 20 and 21,1976.

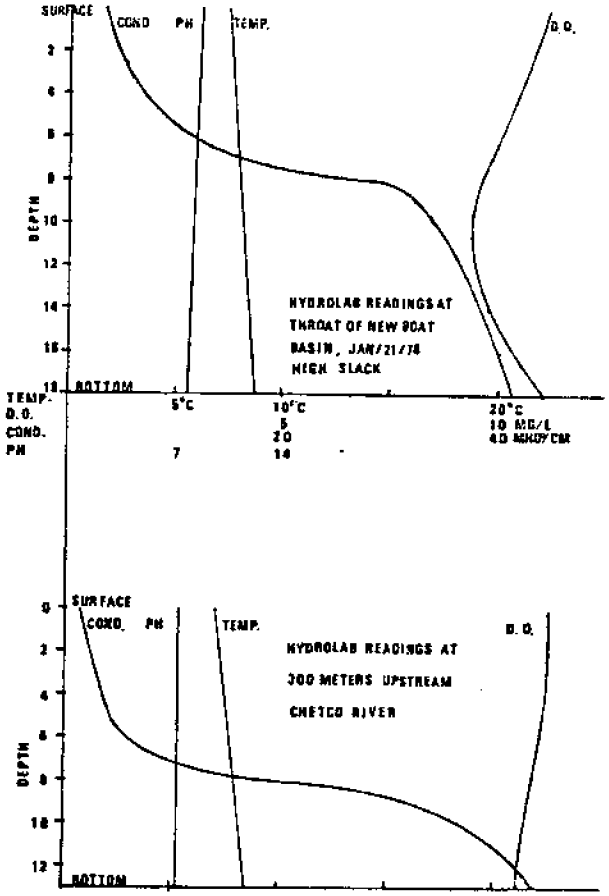

Figure 39. Water quality parameter profiles at the mouth of the new boat basin and entrance to The Chetco River.

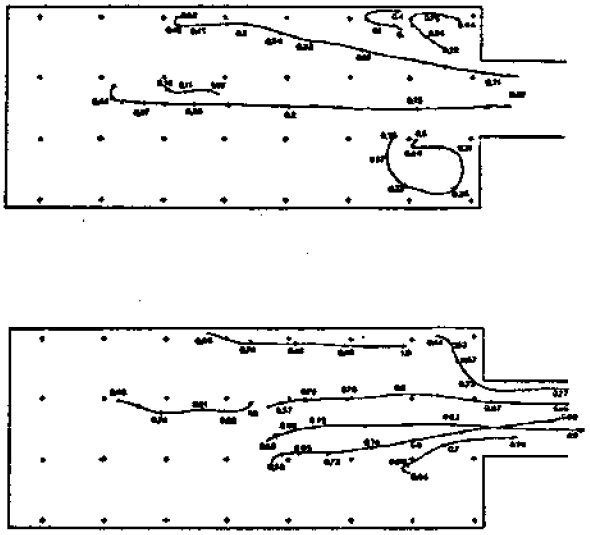

Figure 40. Float pathlines observed in the hydraulic model simulating a 1.83 meter tide and 80 m^3/sec. ambient river runoff.

flushing time obtained from the hydraulic model was 5.7 cycles, 17 ± 3% lower than that determined from the one field experiment. This discrepancy is probably because the diffusion and dispersion mechanisms in the distorted physical model have been exaggerated. An even longer flushing time would be expected for the prototype during the periods of low flow, due to the fact that the field trip happened shortly after a heavy rainfall. Ground water seepage into the basin was noted to be severe while at the same time a creek emptied approximately 1.5×10^{-2} meters/second runoff into the southwest end of the boat basin. These effects combined to cause an increased flushing rate.

Comparisons of dye concentrations found in the laboratory and the field for individual stations are shown in Figure 36. The average dye decay rates between prototype and model were reasonably similar; however, the field results showed dye concentrations at the surface to be higher than those at the bottom, which was opposite to the observations from the hydraulic model. The interpretation of this would be that the dye released in the prototype was less dense than salt water and therefore tended to float on top of the salt water. In the hydraulic model the dye was heavier than the water used in the model, so it tended to sink.

The next task was to check the reproducibility of the hydraulic model for simulation of the current pattern in the boat basin. Drogue studies were carried out in the field. The motions of surface floats and deep drogues (1.8 meters below water surface) were traced over a certain time interval. During the first flooding tide, January 20, 1976, southwest winds were blowing and surface floats followed wind direction. The field study was carried on for the following ebbing and flooding tides. The drogue pathlines during ebbing and flooding tides on January 20, 1976 and during the flooding tide on January 21, 1976 are shown in Figures 37 and 38.

The results of current observations have shown the occurrence of some interesting and unusual conditions. Separation cells existed in the basin. Also, due to the significant salt water intrusion, a pronounced stratified layer existed. (The salinity profiles taken from the mouth of the boat basin and at the river entrance are shown in Figure 39. The vertical profiles of pH, temperature and dissolved oxygen are also shown in this figure.) The deeper drogues proceeded toward the mouth during flooding tide rather than into the basin as the shallow drogues did. The currents observed in the model are shown in Figure 40 for ebbing and flooding tides. The circulation patterns observed in the model depart from those in the prototype since no density difference was reproduced in the model. In order to simulate the circulation patterns due to density differences, salt water intrusion should be properly reproduced in the model.

V. SUMMARY AND RECOMMENDATIONS

In rivers where the lateral boundaries constrain the tidal motion to roughly coincide with the channel centerline, the tidal motion can be adequately and economically reproduced by a one-dimensional tidal dynamic numerical model. The Chetco River fits this situation.

A one-dimensional numerical model using a finite difference scheme was successfully applied to simulate the tides and flows of the Chetco River. After calibration, the numerical model was used to predict the prospective changes of tidal elevation and current after the 1976 boat basin expansion. It was found that the expansion did not affect the tidal hydrodynamic characteristics upstream from the boat basin.

Tides gradually diminish upstream in the Chetco River. The location of the tidal head as well as the tidal prism was found to vary according to the river flow and range of tide. A lag in time between the occurrence of high water at the river mouth and at upstream stations did not occur. In examining the relationship between tide and discharge from computer graphical outputs, it was observed that maximum flow discharge occurs halfway between high and low tide. There was a time lag between maximum flows and currents.

The Chetco estuary was found to be well mixed during periods of low river runoff (summer months and early fall), partially mixed under medium runoff (late spring and fall), and highly stratified during high river runoff. Again, the port expansion was found to not alter the circulation pattern of the estuary.

Flushing studies on the boat basin were carried out using both a hydraulic model and analytical models. The flushing rate of the new boat basin was found to range from four to eight tidal cycles (approximately two to four days) from hydraulic model flushing tests. Circulation cells were observed in the hydraulic model. The size and number of cells depended on the strength of incoming flow.

The conventional tidal prism method was found to overestimate flushing as compared to field measurements. Applying the mixed tank approach for prediction of flushing agreed well with the results from the hydraulic model, although this model did not take ambient conditions into account. Richey's prediction method was compared with traces of float released in the physical model (Figures 31 and 32), and favorable results were observed.

When the field flushing study results were compared with those of the hydraulic and analytical models, both models were found to overestimate the flushing ability of the basin. The geometrically distorted hydraulic model was noted to exaggerate the dispersion and diffusion processes of the system. The invalid assumptions used in the analytical models that the basin water was well mixed and that no water particles would return after leaving the basin are possible explanations for this overprediction.

Water quality studies (Appendix C) indicated that the Chetco River area has satisfactory water quality throughout the seasons. Dissolved oxygen levels closely followed saturation values in the winter and dropped down to 40 percent saturation in the summer, but were still above the range for maintaining good growth and health of fish. The pH ranged between 6.0 and 8.0 and water temperatures were below 10° C all year round. Turbidity data showed that suspended sediments in the river flows were higher in the winter.

Attempts were made to use a two-dimensional finite element numerical model for calculating currents and simulating the circulation in the boat basins. The computer outputs in graphical form are included in Appendix D for a 1.5 meter input tide. Tidal currents are weak, except at the entrance where they were still less that 0.15 m/sec. The inner one third of the basin appeared to never be exchanged. Circulation cells shown in the physical model (Figures 31-34) were not observed in this numerical model, possibly because of the vertical integrated equations formulation.

A two-dimensional numerical model seems to be a useful tool in calculating the flow velocities in boat basins of any shape. However, since marinas are generally small in size on the U. S. Pacific coast, the size of elements for numerical schematization are much too small for economical computer computation. A 56-element system with 41 nodes requires 2540 seconds for a 12.4 hour tidal cycle calculation on CDC 7600. It can be noted that a one layer vertically integrated model will not adequately simulate the circulation in the basin when the density varies significantly over the depth, causing the flow to be stratified.

The study results indicated that generally the tides and ambient flow flushed the new boat basin adequately. An exception to this could occur during dry seasons which coincide with high recreational use of the marina. Engineering actions need to be considered to provide improved performance of marina flushing when these circumstances occur.

It is suggested that possible environmental impacts to estuary systems be carefully examined before approving marina construction. As this study indicates, marina siting is of importance as to its effect on potential changes of estuarine characteristics, strength of tide and ambient currents also govern the circulation patterns in the basin. It is strongly recommended that the present study results be generalized in order to provide general guidelines concerning water quality aspects attendant to marina siting and construction in the Pacific Northwest.

BIBLIOGRAPHY

Abraham, G., Discussion of Thermal and Sewage Pollution in Tidal Estuaries, Paper B-35,IAHR, Istanbul, 1973.

Americal Society of Civil Engineering, Manual of Engineering Practice, No. 25, Hydraulic Models, New York, New York, 1942.

Cameron, W. M. and Pritchard, D. W., Estuarine Circulation Patterns, Proceeding ASCE 81, No. 717, 1955.

Carsten, T., Physical Modeling of Residence Times in Ocean Basins, Proceedings of the 1972 Technical Conference on Estuaries, Oregon State University, Corvallis, Oregon, March 1972.

Daily, J. W. and Harleman, D. R. F., Fluid Dynamics, 1966.

Fisher, H. B. and Holley, E. R., Analysis of the Use of Distorted Hydraulic Models for Dispersion Studies, Water Resource Research, Americal Geophysical Union, Vol. 7, No. 1, February 1971.

Hansen, D. V. and Rattray Jr., M., New Dimensions in Estuary Classification Limnol, Oceanog. 11, 319326, 1966.

Harleman, D. R. F., Physical Hydraulic Models, Chapter V, Estuarine Modeling, An Assessment, E. P. A. Water Quality Office, 1971.

Harleman, D. R. F. and Lee, C. H., The Computation of Tides and Current In Estuaries and Canals, Technical Bulletin No. 16, Committee on Tidal Hydraulics, Corps of Engineers, U. U. S. Army, September 1969.

Harleman, D. F. R. and Thatcher, M. L., The Computation of Tides and Currents in Estuaries and Canals, Technical Bulletin No. 16, Appendix A., Ralph M. Parsons Laboratory, Massachusetts Institute of Technology, Cambridge, Massachusetts.

Holley, E. R. and Karelse, M., Model Prototype Comparisons for Transverse Mixing in Rivers, I. A. H. R., XV Intl.Congress, 1973.

Nece, R. E. and Eugene, P. R., Flushing Characteristics of Small-Boat Marinas, Proceedings, Thirteenth International Conference on Coastal Engineering, Vancouver, B. C., Canada, 1972.

Pearcy, K. L., et. al., Descriptions and information sources for Oregon Estuaries, Water Resources Research Institute, Oregon State University, Corvallis, Oregon, WRRI-19, 1973.

Pritchard, D. W., What is an Estuary?, Physical View Point, Estuaries, Edited by Lauff, G., American Association for the Advance of Science, 1967.

Pritchard, D. W. and Carter, H., Estuarine Circulation Patterns, The Estuarine Environment, Estuaries and Estuarine Sedimentation, Chapter 4, American Geological Institute, Wye Institute.

Richey, E. P., HydroEcological Problems of Marinas in Puget Sound, Proceedings of the 1971 Technical Conference on Estuaries of the Pacific Northwest.

Simmons, H. B., Some Effects of Upland Discharge on Estuarine Hydraulics, Proceedings, A. S. C. E. 81, No. 792, 1955.

U. S. Army Corps of Engineers, District, Draft Environmental Impact Statement, Corps of Engineers Activities in the Chetco, Coquille and Rogue River Estuaries and Port Orford, Oregon, U. S. Army Engineer District, Portland, Oregon, February 1975.

U. S. G. S., Quality of Surface Waters of the United States, U. S. G. S. Geological Survey Water Supply Paper.

Watters, G. Z., Mangleson, K. A., George, R. L., The Hydraulics of Waste Stabilization Ponds, Utah Water Research Laboratory, College of Engineering, March 1973.

Yearsley, J., Unpublished Manuscript, Environmental Protection Agency, 1974.

APPENDIX A. Bathymetric information for the Chetco River and Side Scan Sonar Recordings for the mouth of the Chetco River and boat basin entrance

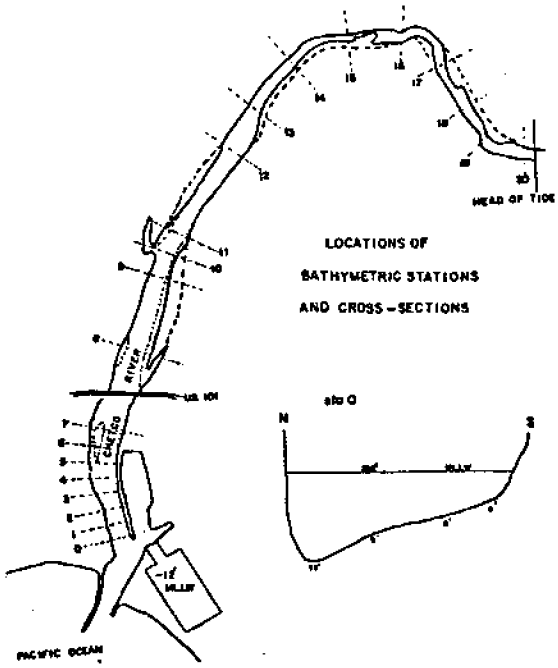

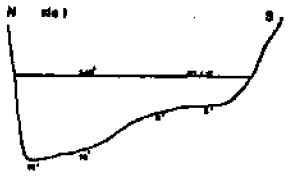

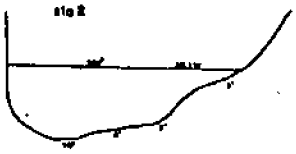

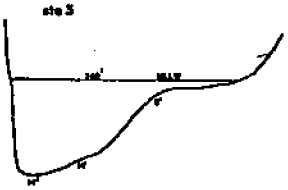

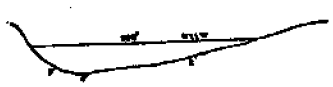

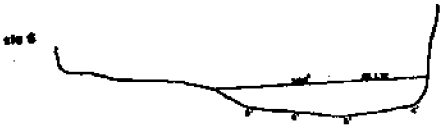

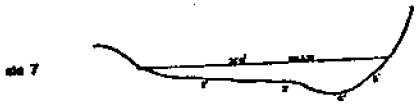

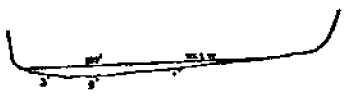

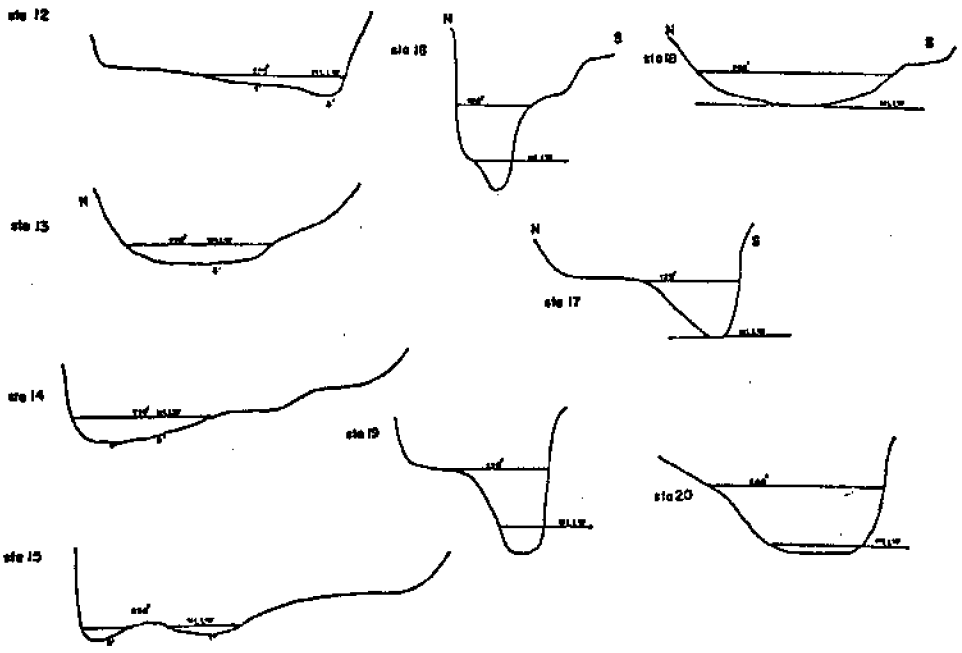
sta 12
sta 16
N
S
sta 18
N
S
sta 13
N
sta 17
N
S
sta 14
sta 19
sta 20
sta 15

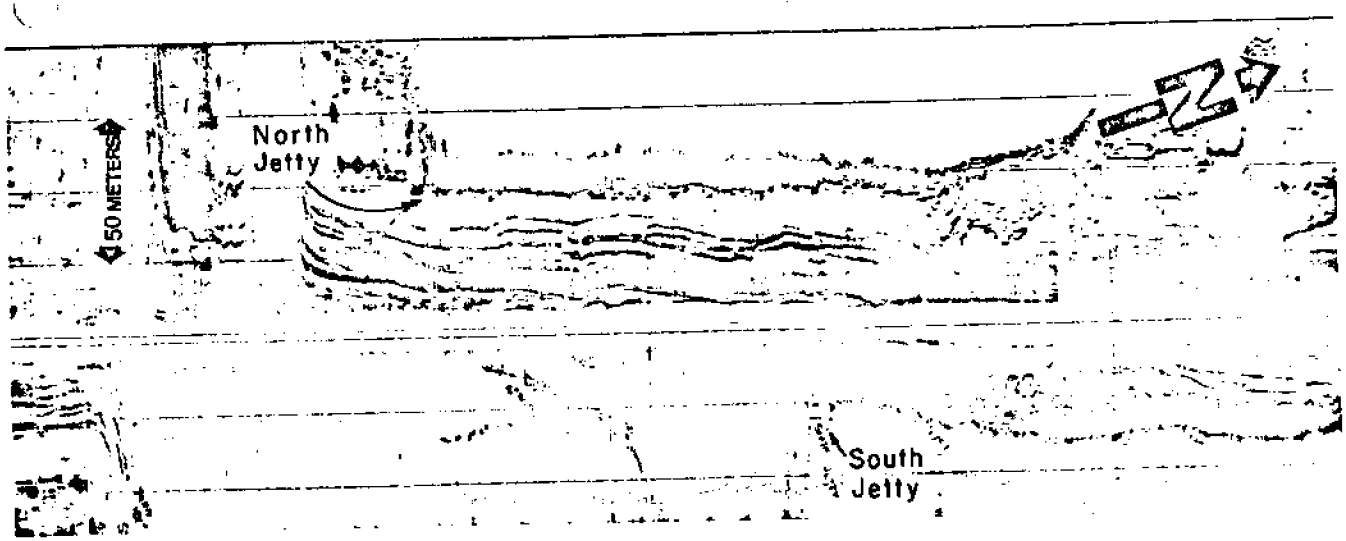
50 METERS
North
Jetty
South
Jetty

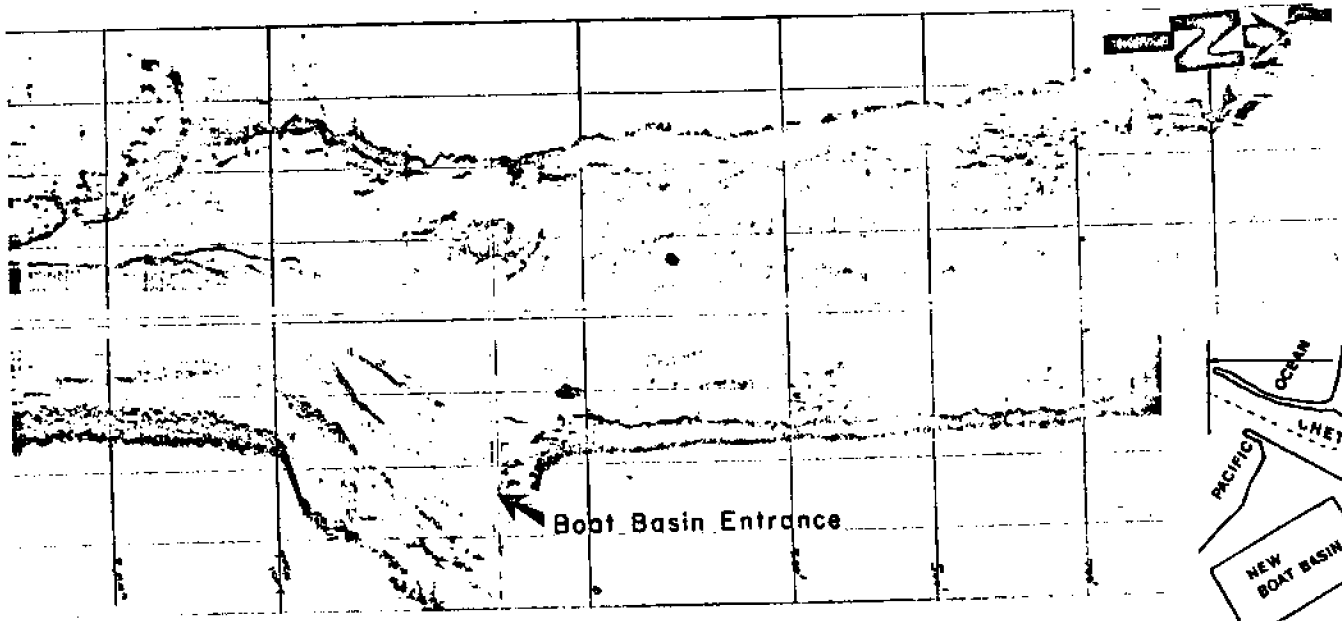
Boat Basin Entrance

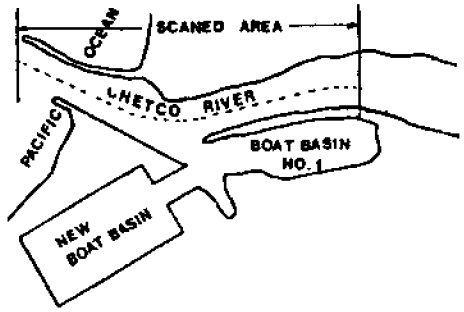
OCEAN
SCANED AREA
NETCO RIVER
PACIFIC
BOAT BASIN
NO. 1
NEW
BOAT BASIN

APPENDIX B. Chetco River schematization for one-dimensional numerical model simulation.

```
* * * * * * * * * * * * * * * * * * * * * * * * * * * * * * * * * * *
*   M.I.T.    TIDAL HYDRAULICS PROGRAM, ONE-DIMENSIONAL SCHEMATIZATION   *
* * * * * * * * * * * * * * * * * * * * * * * * * * * * * * * * * * *
```

SECTION 1. DESCRIPTION OF THE SCHEMATIZED ESTUARY

SOLUTION FOR RIVER INFLOW 300 CFS
TIDAL COMPUTATIONS IN CHETCO ESTUARY JUN, 1977

GEOMETRIC DATA *** OPEN END ESTUARY ***

NUMBER OF STATIONS = 6 ESTUARY LENGTH= 18000 FT.
NUMBER OF TIME INCREMENTS PER PERIOD= [illegible] PERIOD= [illegible] SECONDS

CASE 2. IRREGULAR CROSS-SECTION (STORAGE)

MILES	[illegible]	[illegible]	B	[illegible]	FEET	SECTION
0	14.[illegible]	9.[illegible]	540.0	350.0	0	1
.68182	6.52[illegible]	17.[illegible]	420.0	420.0	3600	2
1.36364	4.5[illegible]	19.[illegible]	400.0	400.0	7200	3
2.04545	4.15[illegible]	19.[illegible]	350.0	330.0	10800	4
2.72727	1.5[illegible]	22.[illegible]	300.0	300.0	14400	5
3.40909	1.15[illegible]10	29.[illegible]5000	300.0	300.0	18000	6

SECTION 2 CHANNEL ROUGHNESS AND WIND EFFECTS

CASE 1 CONSTANT ROUGHNESS AND CONSTANT WIND

NO WIND

MILES	MANNING	FD	V	PHI	FEET	SECTION
0	.0250000	0	0	0	0	1
.68182	.0250000	0	0	0	3600	2
1.36364	.0250000	0	0	0	7200	3
2.04545	.0250000	0	0	0	10800	4
2.72727	.0250000	0	0	0	14400	5
3.40909	.0250000	0	0	0	18000	6

SECTION 3. SURFACE ELEVATION AT THE ENTRANCE

MWL 0 FT ABOVE MSL AT OCEAN
MSL 26.00 FT ABOVE THE HORIZONTAL DATUM

INITIAL CONDITIONS ALL FROM CARDS

```
TIDAL CYCLE    1        0 HOURS      DAY    0        0 HOURS
STATIONS    1       3          5
ELEV.           0          0          0

TIDAL CYCLE    1      .028 HOURS      DAY    0      .028 HOURS
STATIONS       2          4          6
DISCHARGE          0          0          0
```

APPENDIX C. Water Quality Data obtained from the Chetco River and boat basin areas. Water quality data were collected in the Chetco River and boat basin areas in 1975 1976 to provide base line information for characterizing the water quality of the area. Measurements included in-situ data collected with the Hydrolab Water Quality Monitor and bottle samples which were subsequently in the laboratory. Parameters which were measured included conductivity, temperature, dissolved oxygen, pH and turbidity. The water quality sampling stations are shown in Figure C-1, followed by measured data presented in tabular form.

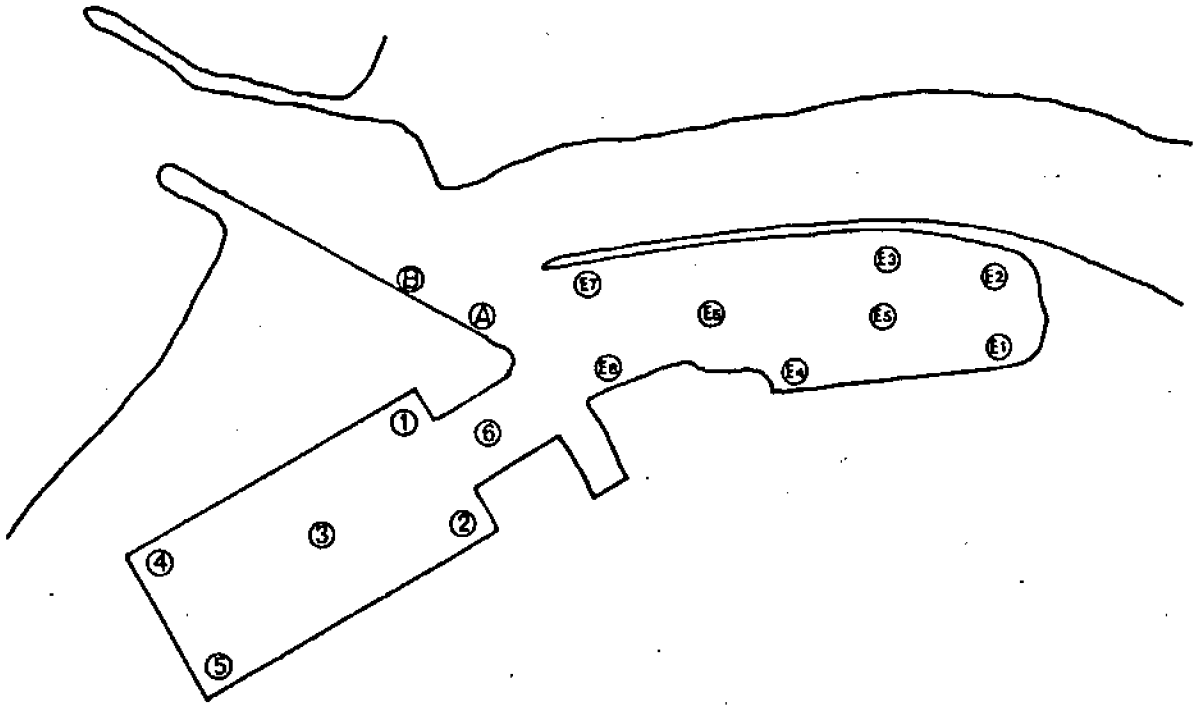

Figure C-1 Water quality sample station identification

FOLD LINE

Use BLACK Typewriter Ribbon SINGLE SPACE COPY

Appendix C. Water Quality Data

Station	HYDROLAB Time Feb 8 '75	Depth (m)	Temp. (°C)	DO (ppm)	Sal (°/oo)	pH	BOTTLE SAMPLE Time Feb 9 '75	Depth	DO (ppm)	pH	Tur(JTU)	SAL(°/oo)
E2	11:30 am	1.5m	6.5	11.5	0.4	7.2	10:49 am	0	12.2	*	40	-
	12:00 am		6.5	11.5	0.4	7.2	10:54 am	1.5	11.0	*	25	-
	13:00 pm		6.5	11	0.4	7.0	10:58 am	3.9	12.2	*	35	-
	14:30 pm		6.5	10.5	0.5	7.0						
E7	15:00 pm		6.8	10.8	0.4	7.0	11:25 am	0	11.9	*	25	-
	18:00 pm		6.8	10.5	0.5	7.0	11:28 am	1.5	11.8	*	27	-
	23:00 pm		6.8	10.6	0.5	7.2	11:35 am	6.0	11.9	*	58	-
	Feb 9 '75											
	3:00		6.8	10.5	0.5	7.1						
	6:00		6:8	10.6	0.5	7.0						
	8:00		6.8	10.8	0.5	7.0						
	Sept 15 '75	mid										
	13:00		9.4	7.0	42	7:8						
	15:00		9.5	6.2	44	7.8	16:30	5.5	7.6	7.7	7.0	31.43
	17:00		9.5	7.0	43	7.9						
	19:00		9.5	7.2	42	7.8						
	20:30		*	7.8	42	7.8						
	21:30		*	6.6	40	7.8						
	22:00		*	6.2	42	7.8						
	Sept 16 '75											
	24:00		*	7.0	42	7.9						
	2:00		*	6.0	40	7.9						
	4:00		*	5.8	44	7.8						
	6:00		*	6.6	46	7.9						
	8:00		*	6.6	45	7.6						
	10:00		*	7.2	42	7.8						
	12:00		*	7.2	42	7.8						
	14:00		*	6.2	43	7.7						
	16:00		*	6.2	42	7.7						

Appendix C. Continued

Station	Time	HYDROLAB Depth (m)	Temp. (°C)	DO (ppm)	Sal (°/oo)	pH	BOTTLE SAMPLE Time	Depth	DO (ppm)	pH	Tur(JTU)	SAL(°/oo)
	Jan 19 '76											
	19:00	1.2 m	6.8	9.5	7.5	7.5						
	21:00		6.6	10.0	5.2	7.5						
	23:00		6.6	10.0	2.8	7.2						
	Jan 20 '76											
	1:00		6.6	10.0	3.6	7.2						
	3:00		6.5	10.0	4.0	7.9						
	5:00		6.5	10.1	3.0	7.5						
	9:00		6.2	10.2	3.8	7.5						
	12:00		6.5	10.0	4.0	7.2						
	13:00		6.5	9.8	6.8	7.0						
	15:00		7.0	10.2	6.2	7.6						
	17:00		6.8	10.1	7.6	7.8						
	Jan 21 '76											
	11:12		7.4	10.4	6.3	7.5						
	12:30		7.0	10.0	7.5	7.5						
	13:00		7.0	9.8	7.6	7.4						
E1							Feb 9 '75					
							10:30	0	11.7	-	42	-
							10:37	115	11.8	-	40	-
							10:43	3	11.7	-	41	-
							Sept 18 '76					
							16:15	2.5	6.2	7.6	20	30.6
							Jan 21 '76					
							13:00	2.5	9.5	6.8	3.4	18
E3							Feb 9 '75					
							11:12	0	12.4		12.4	78
							11:15	1.5	12.0		24	
							11:19	5.5	12.4		22	

Appendix C. Continued

Station	HYDROLAB Time	Depth (m)	Temp. (°C)	DO (ppm)	Sal (°/oo)	pH	BOTTLE SAMPLE Time	Depth	DO (ppm)	pH	Tur(JTU)	SAL(°/oo)
E4							Feb 9 '75					
							11:52	0	11.6		19	
							11:57	3.0	11.7		47	
							12:00	4.5	12.8		50	
E8							12:08	0	11.6		18	
							12:12	3.0	12.1		51	
							12:15	5.5	12.1		52	
							Jan 21 '76					
1							10:50	surface	11	6.0	8.8	2.6
								bottom	11	6.3	11	6.7
2							10:52	surface	10.1	6.5	14	3.5
								bottom	9.0	6.2	11	7.7
3							10:55	surface	11.8	6.3	5.0	2.1
								bottom	9.2	6.0	1.5	9.3
4							11:00	surface	10.7	6.8	1.4	-
								bottom	8.3	6.5	8.8	17
S							11:10	surface	11.3	6.4	10	-
								bottom	9.5	6.3	11	13
E6							11:15	surface	11.5	6.8	4	-
								bottom	9.5	6.3	11	13
E5							11:30	surface	11.4	6.2	7.0	-
								bottom	7.7	7.5	1.7	22.4
B							11:20	surface	11	7.3	3.4	-
								bottom	7.4	7.1	7.0	18.9
C							13:00		*	7.2	3.0	0
E2							11:35	surface	11.5	6.5	9.5	-
								bottom	9.5	6.8	3	17
A							Feb 9 '75					
							12:00	surface	12.1	*	*	*
B							12:00	surface	12.1	*	*	*
							Sept 18 '75					
							16:15	1.2 m	10.6	8.1	20	25.4

Appendix C. Continued

		HYDROLAB					BOTTLE SAMPLE				
Station	Time	Depth (m)	Temp. (°C)	DO (ppm)	Sal (°/00)	pH	Depth	DO (ppm)	pH	Tur (JTU)	Sal(°/100)
	Sept 2 '76										
3	15:13	3.7	14	8.1	44.0	7.8		8.8		8.3	
		1.8	14.5	7.9	43.0	7.7					
		0.6	15.0	7.6	34.0	7.7		9.0		3.0	22.9
5	15.22	3.9	14.0	7.6	45.0	7.0					
		2.0	14.0	8.0	43.5	7.8					
		0.6	15.0	7.9	37.0	7.7					
6	15.03	4.9	14.0	8.2	45.0	7.8		9.2		3.5	32.9
		2.4	14.0	8.2	44.0	7.8		9.4		1.3	31.64
		0.6	15.0	7.8	35.0	7.7		9.2		3.0	18.27
E2	14.19	5.2	14.0	6.7	46.0	7.6		7.0		7.5	30.45
		2.6	14.0	8.0	46.0	7.8		9.5		10.0	27.65
		0.6	16.0	7.4	32.0	7.7		9.5		5.0	17.5
E6	14.39	4.9	14.0	7.8	45.0	7.7		9.5		9.5	
		2.4	14.0	8.3	46.0	7.8		6.0		9.8	31.85
		0.6	15.5	7.4	35.0	7.7		2.4		9.1	
E8	14:54	3.4	14.0	8.4	46.0	7.8					
		1.7	14.0	8.4	45.0	7.8					
		0.6	16.0	7.7	30.0	7.7					
B	14:10	1.8	14.5	8.6	46.0	7.8				10	29.4
		0.9	15.5	8.0	39.5	7.7		9.0		10	24.5
		0.6	16.0	7.3	35.0	7.6		8.0		8.5	18.55

APPENDIX D. Computer output of a finite-element numerical model applied to the new boat basin.

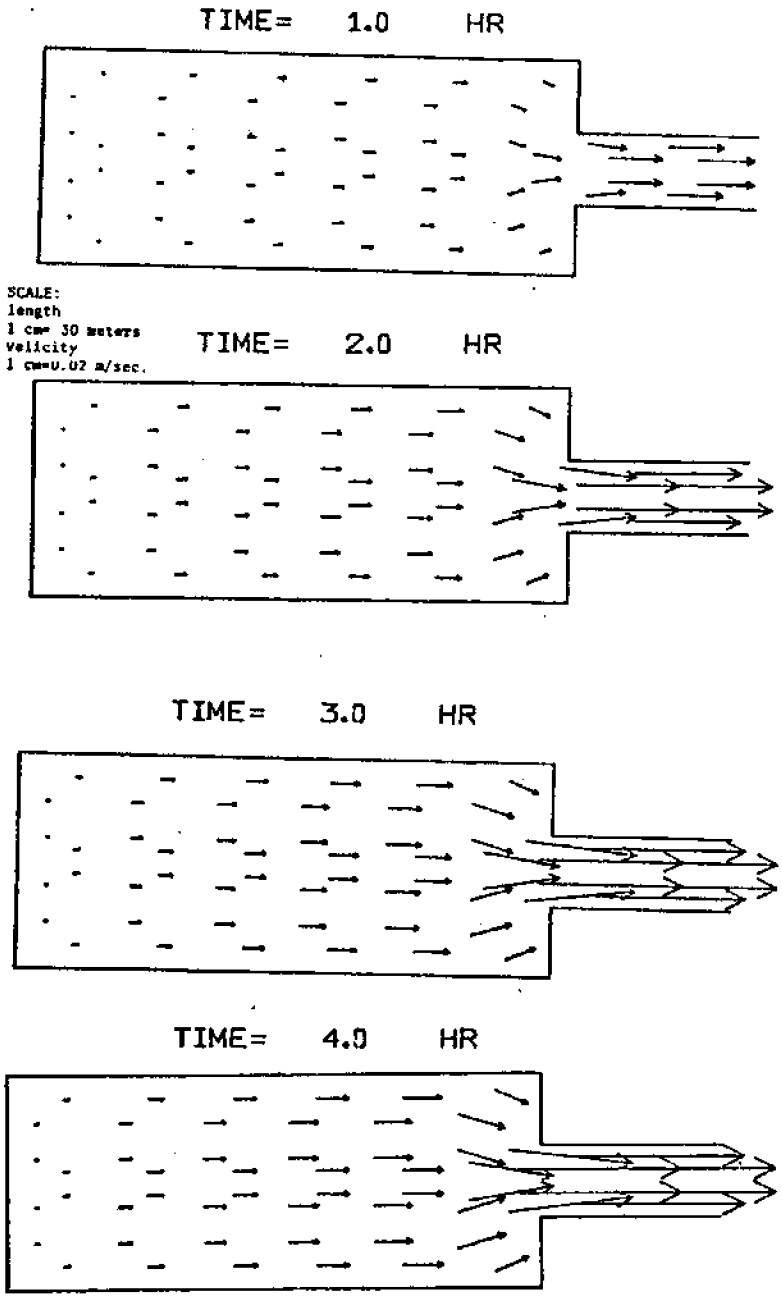

FOLD LINE

TIME= 5.0 HR

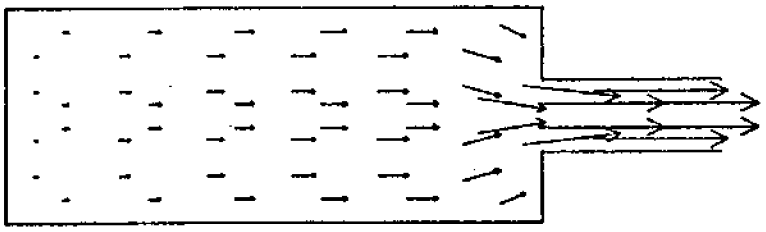

TIME= 6.0 HR

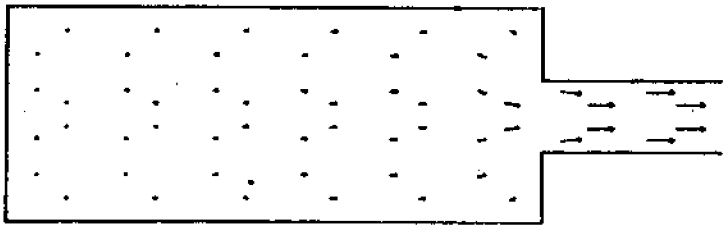

TIME= 7.0 HR

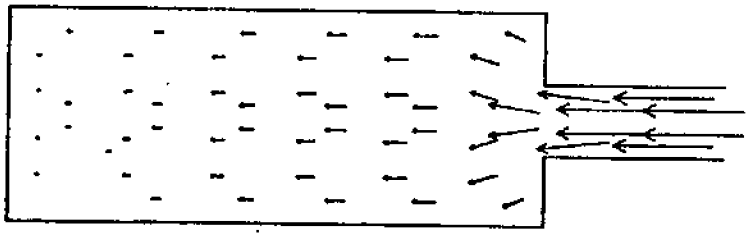

TIME= 8.0 HR

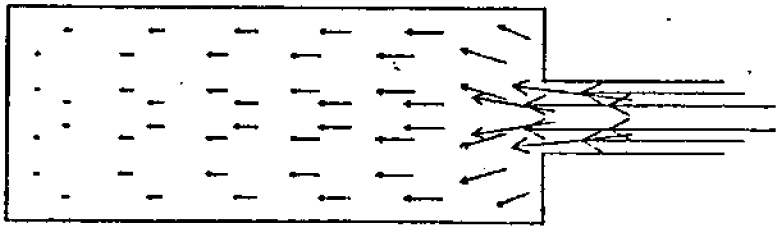

TIME= 9.0 HR

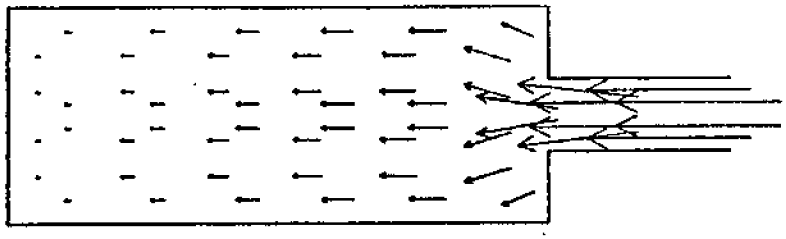

TIME= 10.0 HR

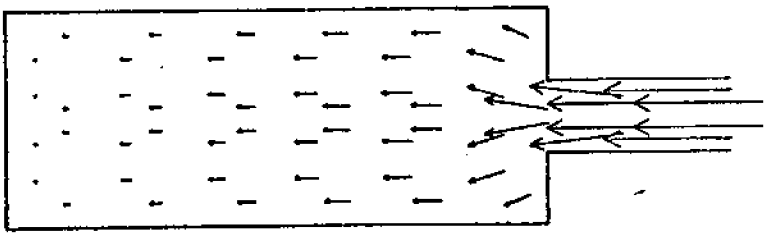

TIME= 11.0 HR

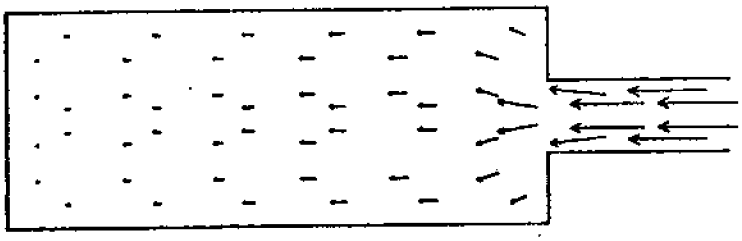

TIME= 12.0 HR